Schweizerische Eidgenossenschaft
Confédération suisse
Confederazione Svizzera
Confederaziun svizra

Federal Department of the Environment, Transport,
Energy and Communications DETEC

Swiss Federal Office of Energy SFOE
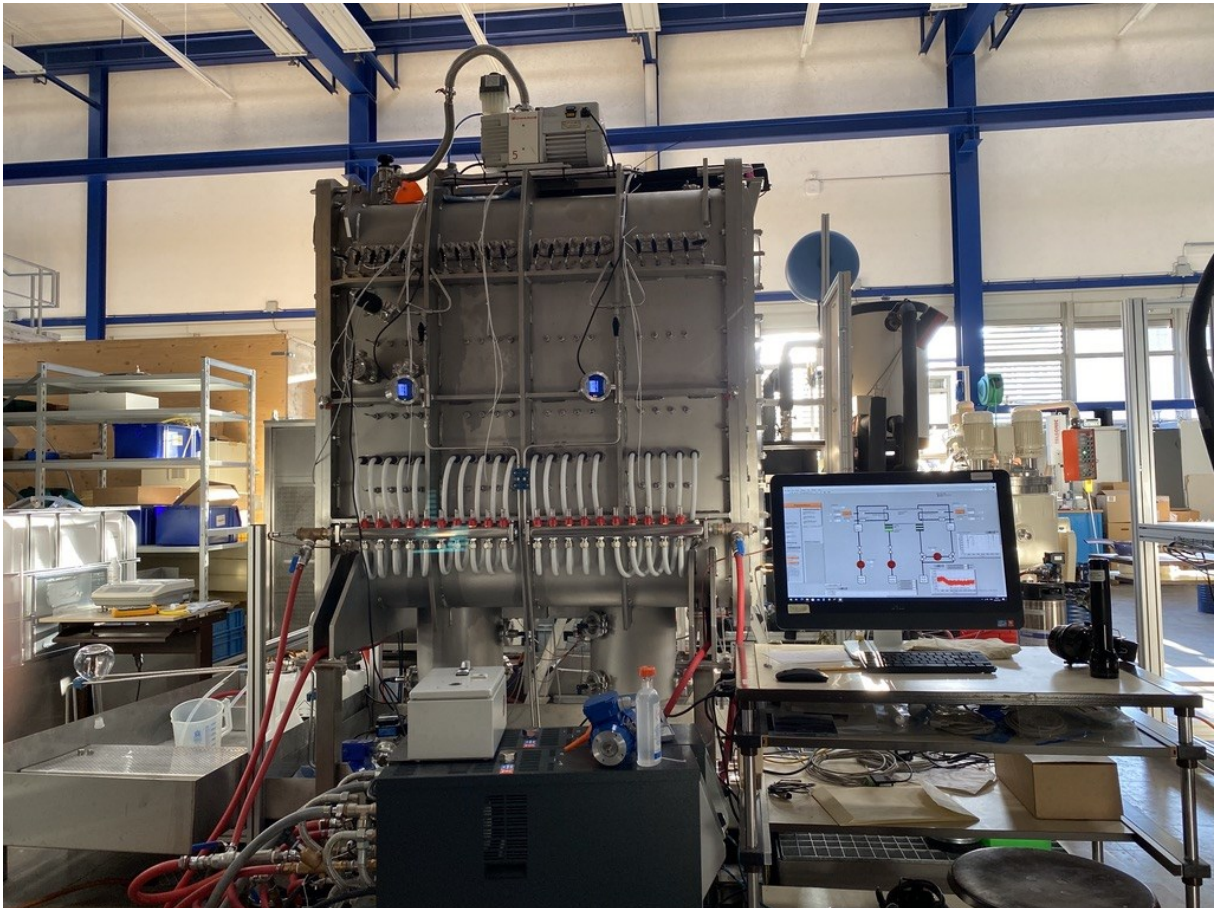Energy Research and Cleantech Division

Final report dated 09.06.2023

Development of a liquid sorption based long term thermal energy storage demonstrator

Source: HSLU©Fumey 2022

Date: 01.06.2023

Location: Horw

Authors:
Benjamin Fumey (Empa), HSLU, benjamin.fumey@hslu.ch
Luca Baldini (Empa), ZHAW, luca.baldini@zhaw.ch
Robert Weber, Empa, robert.weber@empa.ch

The authors bear the entire responsibility for the content of this report and for the conclusions drawn therefrom.

Zusammenfassung

In diesem Projekt wurde an der Empa und der HSLU ein Langzeit-Wärmespeicher-Demonstrator auf der Basis eines Flüssigsorptionsverfahrens entwickelt und im Labor der HSLU getestet.

Untersucht wurde die Absorption von Wasserdampf (Absorbat) in wässrigem Natriumhydroxid (Absorbens). Sowohl die Raman-Spektroskopie zur Messung des Massentransports des Absorbats im Absorbens als auch die Neutronenbildgebung zur Visualisierung der Aufnahme wurden eingesetzt. Es wurde festgestellt, dass der Massentransport langsam ist und eine Beschleunigung durch den auftriebskraftverstärkten Transport gefunden werden kann.

Auf der Grundlage der Ergebnisse der Materialanalyse wurde ein neuartiges Design für den Wärme- und Massenaustausch entwickelt, bei dem ein herkömmliches, vertikal installiertes Spiralrippenrohr verwendet wird. Das Design profitiert vom Gegenstrom-Wärmeaustausch, der langen Expositionszeit des Absorbens und der Entladung in einem Durchgang. Es wurde ein Prüfstand für einen Einrohr-Wärme- und Stofftauscher im Labormaßstab gebaut, und die neue Idee wurde mit verschiedenen Abmessungen und Materialien getestet.

Auf der Grundlage dieser Bewertung wurde ein Sorptionswärmespeichersystem im Maßstab für ein Einfamilienhaus gebaut, indem mehrere Spiralrippenrohre parallel geschaltet wurden. Das System wurde mit großen Speichertanks gekoppelt, die 1200 kg wässrige Natriumhydroxid enthalten, und sowohl für die Absorption als auch für die Desorption getestet. Unter allen Testbedingungen wurde ein stabiler Betrieb erreicht und eine Nennleistung von 4 kW sowie eine Energiedichte von 200 kWh/m3 erzielt.

Résumé

Dans ce projet, un démonstrateur de stockage d'énergie thermique à long terme basé sur un processus de sorption liquide a été développé à l'Empa et à la HSLU et testé dans le laboratoire de la HSLU.

L'absorption de vapeur d'eau (absorbat) dans de l'hydroxyde de sodium aqueux (absorbant) a été étudiée. La spectroscopie Raman a été utilisée pour mesurer le transport de masse de l'absorbat dans l'absorbant et l'imagerie neutronique pour visualiser l'absorption. Il a été constaté que le transport de masse est lent, et l'accélération peut être trouvée par la force de flottabilité améliorant le transport.

Sur la base des résultats de l'analyse des matériaux, une nouvelle conception d'échange de chaleur et de masse a été développée en utilisant un tube à ailettes en spirale conventionnel installé verticalement. Cette conception bénéficie d'un échange de chaleur à contre-courant, d'une longue durée d'exposition de l'absorbeur et d'une décharge à passage unique. Un banc d'essai d'échangeur de chaleur et de masse à tube unique à l'échelle du laboratoire a été construit, et la nouvelle idée a été testée avec une variation des dimensions et des matériaux.

Sur la base de cette évaluation, un système de stockage de chaleur par sorption à l'échelle d'une maison individuelle a été construit en connectant plusieurs tubes à ailettes en spirale en parallèle. Le système a été couplé à de grands réservoirs de stockage contenant 1200 kg d'hydroxyde de sodium aqueux et testé pour l'absorption et la désorption. Un fonctionnement stable a été obtenu dans toutes les conditions d'essai et une puissance nominale de 4 kW et une densité énergétique de 200 kWh/m3 ont été atteintes.

Summary

In this project, a long-term thermal energy storage demonstrator based on a liquid sorption process was developed at Empa and HSLU and tested in the HSLU laboratory.

The absorption of water vapor (absorbate) in aqueous sodium hydroxide (absorbent) was investigated. Both Raman spectroscopy to measure the mass transport of the absorbate in the absorbent and neutron imaging to visualize the uptake were used. It was found that the mass transport is slow, and acceleration can be found by buoyancy force enhanced transport.

Based on the material analysis results, a novel heat and mass exchange design was developed using a conventional spiral fin tube installed vertically. The design benefits from countercurrent heat exchange, long absorber exposure time, and single-pass discharge. A laboratory scale single tube heat and mass exchanger test rig was built, and the novel idea was tested with a variation of dimensions and materials.

Based on this evaluation, a single-family home scale sorption heat storage system was built by connecting multiple spiral fin tubes in parallel. The system was coupled to large storage tanks containing 1200 kg of aqueous sodium hydroxide and tested for both absorption and desorption. Stable operation was achieved under all test conditions with a nominal power output of 4 kW and an energy density of 200 kWh/m3.

Main findings

- The spiral finned tube heat and mass exchanger functions well for liquid sorption heat storage. High energy density requires long exposure time to reach high concentration change. The spiral finned tube approach enables long exposure time with good wetting and counterflow heat exchange.

- Buoyancy forces can be employed to increase mass transport.
  Absorption kinetic is limited by mass transport from the sorbent surface to the fluid bulk. Since the discharged absorbent density is lower than the charged, this characteristic can be used to move charged sorbent to the absorption surface.

- Maximum performance is reached at minimum required temperature gain.
  Due to the concentration dependent temperature gain, the temperature to heat relation in absorption is not linear, more heat is available at lower temperatures. Thus, maximum discharging requires minimum temperature gain.

Contents

1   Introduction

1.1   Background information and current situation

Thermal energy storage is considered an important enabler for the full utilization of renewable energy in buildings [1-6]. Critical parameters for success are high energy density, low loss during storage time [7] and low storage cost [8]. Sensible, latent and sorption storage technologies are investigated [9]. Sensible and latent storage systems are subject to continuous heat loss, a major issue for long term storage. This is countered by large-scale sensible storage systems [10] and subcooling in latent systems [11,12]. Sorption storage, on the other hand, is based on a modification of the sorption heat pump with intermitting working pair storage [9]. Thus, the potential (work) to recover heat at increased temperature is stored instead of storing sensible heat [13]. Key competitive advantages of this approach are its potentially high energy density (up to 6 times that of equivalent water-based systems) and its lack of potential loss over time, as recombination of the separated media is prevented [7,14]. For this reason, a specific application that is being focused on is inter-seasonal heat storage for residential space heating [1,15].

Sorption heat storage follows the concept of a reversible decomposition reaction process. Both thermophysical and thermochemical bonds are included [16,17]. In a bidirectional temperature swing process [18], an aggregate change of the sorbate because of evaporation and condensation is incorporated [13, 19-24]. Desorption and condensation (charging) and evaporation and sorption (discharging) are separated in time, with the working pair stored in both charged and discharged state [13, 25-27]. Processes of adsorption onto solid sorbents [17,28,29] and sorption into solid or liquid sorbents [17,18,25,29,30] are considered. By preventing sorbent and sorbate recombination, the sorption potential can be stored indefinitely, provided the pot life of the material is granted. The solid materials studied include zeolites, silica gels, and salts, as well as the former impregnated with salt, referred to as composite materials. Liquid absorbents studied are usually alkaline aqueous solutions such as sodium hydroxide, calcium chloride, and lithium bromide [31-36]. Generally, water is used as a sorbate because it has a high heat uptake/release in the gas liquid phase change, but generally limits the heat input to temperatures above 0 °C. Other sorbates considered are ethanol and methanol, and ammonia absorbed in water.

There are four different types of processes found in sorption storage systems. These are open and closed, and fixed and transported [37]. Open vs. closed refers to the exposure of the sorbent to the air. Open processes exchange heat and matter (water vapor) with the environment [13,18,38-42], while closed processes take place in a vapor environment, usually at subambient pressure, and exchange only heat with the surrounding [13,44,45]. Fixed vs. transported refers to the handling of the sorbent. In the fixed process, the sorbent is stationary and connected to the sorber/desorber heat and mass exchanger (HMX) [13,18,34,41,45,46], whereas in the transported process, the sorbent is moved from storage vessels to the sorber/desorber HMX and back [13,31,34,44,47-49]. In general, the fixed process is used for solid sorbents, while liquid sorbents are transported (pumped). Systems using the transport method have a continuous, uniform power output at a constant temperature, whereas in fixed bed systems this varies greatly depending on the state of charge [37]. Research in this area began in the early 1960s [50,51] and continues [52-55], although mature systems are still lacking [56].

This project dealt with the development of a long-term thermal energy storage system based on the process of water absorption in aqueous sodium hydroxide for heating buildings. This research area was initiated at Empa in 2002 and has been supported over the years by both Swiss federal and European research funding, and was taken over by the HSLU in the course of this project.

In this work, the development of a suitable heat and mass exchanger to facilitate water absorption in sodium hydroxide was undertaken based on previous research . Initially, a plate-type design was proposed with aqueous sodium hydroxide on the plate and a double bottom to channel the heat transfer fluid [57]. Desorption was possible, but not absorption. In another approach, a tube bundle

heat and mass exchanger was built, following the common sorption heat exchanger design. Again, absorption was not successful due to poor wetting and short exposure time [58].

From this work, it was recognized that although the sorption heat storage process is similar to the sorption heat transformer (chiller, heat pump), due to the inclusion of sorbent and sorbate storage (energy capacity), a fundamental rethinking of the heat and mass exchanger design was required. This work and the resulting upscaling has been done in this project.

1.2   Purpose of the project

The purpose of this project was to develop a novel heat and mass exchanger design for liquid absorption heat storage based on aqueous sodium hydroxide that performs well in both desorption and absorption, and from this to provide a functional application scale technology demonstration for building heating to advance the technology readiness level.

1.3   Objectives

The overall objective of this project was to achieve good functionality of a single-family home scale sorption heat storage demonstration system to demonstrate the technical feasibility and application potential of storing renewable energy from summer to winter for building heating.

The use of aqueous sodium hydroxide as absorbent and water as absobate for sorption heat storage was investigated. Theoretical evaluation so far has shown that charging can be done by solar thermal collectors (75°C) and the discharge temperature is sufficient for space heating (35°C). Volumetric energy densities of 250kWh/m3 to 350kWh/m3 (4 to 5 times that of water) can be achieved, and no loss occurs during storage. In addition, the moderate material price seems to favor low-cost energy storage.

Given the aforementioned challenges, a thorough, application-specific, in-situ study focused on the uptake and release of water from aqueous sodium hydroxide was required to characterize the process. It was anticipated that by gaining insight into the mass transport of absorbate to and from the surface of the absorbent, bottlenecks and potential methods of improvement could be identified.

Based on this knowledge, a new heat and mass exchanger design was to be researched and developed. This was to be tested on a small physical and performance scale and then scaled up to a performance in the range of a single-family home. Extension of the upscaled heat and mass exchanger with aqueous hydroxide and water storage tanks was then planned to take the first steps towards a comprehensive sorption heat storage system for buildings and to provide proof of technology functionality. The physical work was accompanied by system-level simulation to provide an indication of performance in buildings.

The quantitative project targets for the single family home scale system were:

- 5 kW thermal discharge power
- 150 - 200 kWh/m^3 energy density

Description of facility

One method of reducing building energy demand in winter is seasonal energy storage, which stores energy from summer (surplus) to winter (deficit). In Switzerland, 80% of building energy consumption is used for space heating and hot water [59]. For this reason, thermal energy storage can be effective, with the prospect of much lower storage costs than electrical storage. A building with seasonal energy storage will make a positive contribution to energy security by reducing the load on the electricity grid in winter, and to the reduction of greenhouse gas emissions by using renewable and CO_2-free energy.

Based on the low number of charge and discharge cycles and the resulting long storage time, the two basic challenges for long term storage are price and loss per storage time. The absorption of water on aqueous sodium hydroxide has prospect for both, sodium hydroxide is a low-cost chemical, and lossless storage is achieved by strict separation of water and aqueous sodium hydroxide.

Sorption heat storage with aqueous sodium hydroxide is based on a temperature swing process. During loading, aqueous sodium hydroxide with a concentration below 50 wt% (initial concentration) is heated and water is evaporated to increase the solution concentration to 50 wt% (solidification barrier). Both substances are stored separately in the liquid state. In the discharge (heat release) process, water vapor is generated from the stored water and low-temperature heat and is absorbed on the charged sorbent, accumulating the heat of condensation (temperature increase) to the concentration and vapor pressure dependent equilibrium. Figure 1 shows the process of desorption (dashed line) and absorption (solid line).

The storage performance is evaluated in respect to temperature gain (output temperature), heat and mass exchanger power and energy density. The temperature gain depends on the concentration, power on the heat and mass transport kinetics and energy density on the concentration difference between charged and discharged state. For this reason, the process of absorption must occur in a single absorbent pass and sufficient time for maximum absorate uptake must be possible.
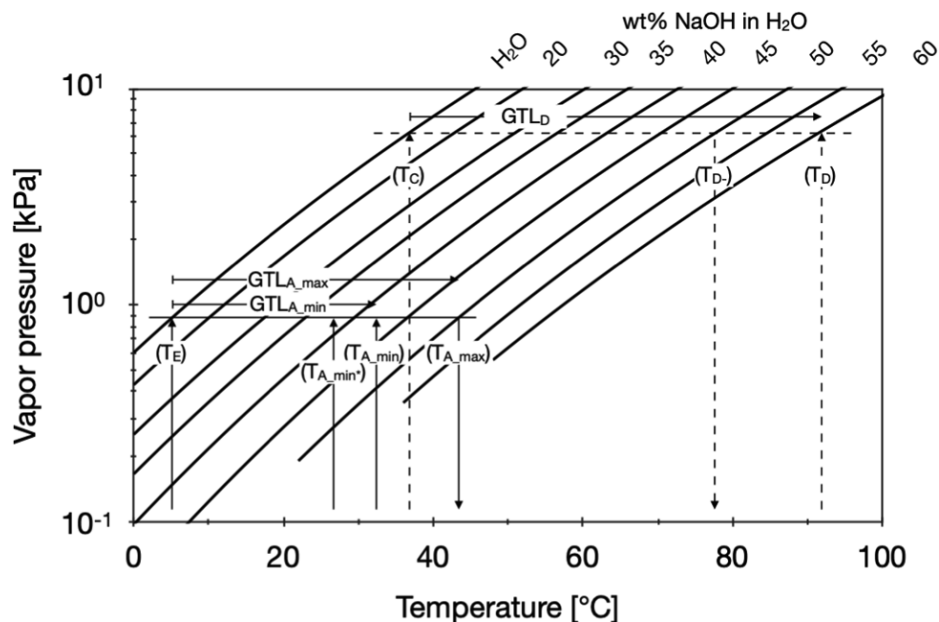

Figure 1: Vapor pressure vs temperature diagram of NaOH at varying concentrations.

This project built several facilities to study absorption, develop the novel heat and mass exchanger, and scale up to a single-family home demonstrator. A stepwise approach was followed from material study to system development including:

- To evaluate the heat and mass transport limitations in absorption and desorption, the water mass transport from the absorber surface to the film bulk, measured in-situ by Raman spectroscopy under application specific conditions, was analyzed. It was recognized that mass diffusion is performance limiting.
  This work was published in: Fumey, B., Baldini, L. and Borgschulte, A., "Water Transport in Aqueous Sodium Hydroxide Films for Liquid Sorption Heat Storage", Energy Technol., Volume 8, 2020, 2000187.

- Using neutron imaging, surface-to-bulk mixing, a method of mass transport enhancement was analyzed in an attempt to find solutions to overcome mass diffusion limitations. Strong buoyancy forces from concentration gradients were detected and a method to exploit them developed.
  This work was published in: Fumey B., Borgschulte A., et al. Enhanced gas-liquid absorption through natural convection studied by neutron imaging, International Journal of Heat and Mass Transfer 182 (2022) 121967

- Based on the results, a novel HMX design was pursued to meet the requirements of the heat storage application. The challenges are: long exposure time, countercurrent process, single pass, and avoidance of absorbent accumulation. A solution was found based on a vertically installed spiral fin tube and a laboratory-scale heat and mass exchanger was built and tested.
  This work was published in: Fumey B., Weber R., Baldini L., Liquid sorption heat storage – A proof of concept based on lab measurements with a novel spiral fined heat and mass exchanger design, Applied Energy, Volume 200, 2017, 215-225

- In a final step, an upscaled sorption heat storage system was designed, built and extensively tested with more than 400 hours of operation and 6 charge and discharge cycles of 1200kg of aqueous NaOH.
  This work is under publication.

- In parallel, simulation work was performed, based on early lab-scale reactor results, to predict the operational performance of this storage system in a single or multi-family dwelling under varying climatic conditions.
  This work is under publication.

1.4 Raman spectroscopy mass transport analysis cell

To gain insight into the uptake (transport from the surface to the bulk) and release (transport from the bulk to the surface) of water from aqueous sodium hydroxide under heat storage application conditions, a test cell was constructed to fit the Raman spectroscopy facility at Empa. Figure 2 shows an illustration of the cell and Figure 3 an image of the setup.

The test facility was designed to realistically mimic the water exchanger from the gas to the liquid interface, expected in a technical heat and mass exchanger. The cell was constructed of a stainless-steel body with a central round compartment and a glass covering. The compartment contained a Peltier element with a stainless-steel sheet cover to support an absorbent droplet (thin film).
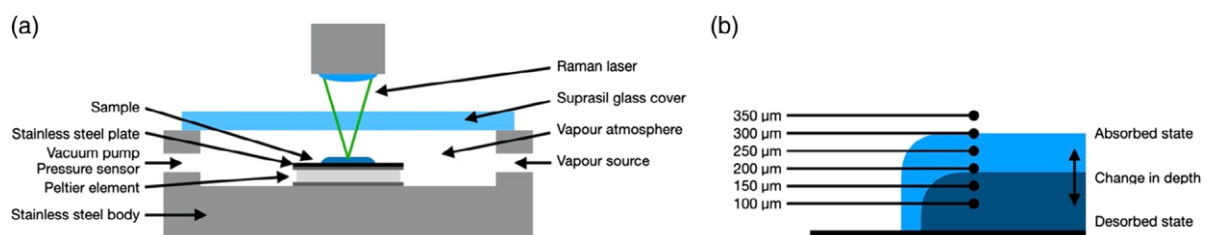
Figure 2: Test cell setup. a) Illustration of the setup with the Peltier cooler and heater, stainless-steel plate, and sample. b) Illustration of the Raman depth profiling upon moving the focal point into or out of the aqueous sodium hydroxide film.
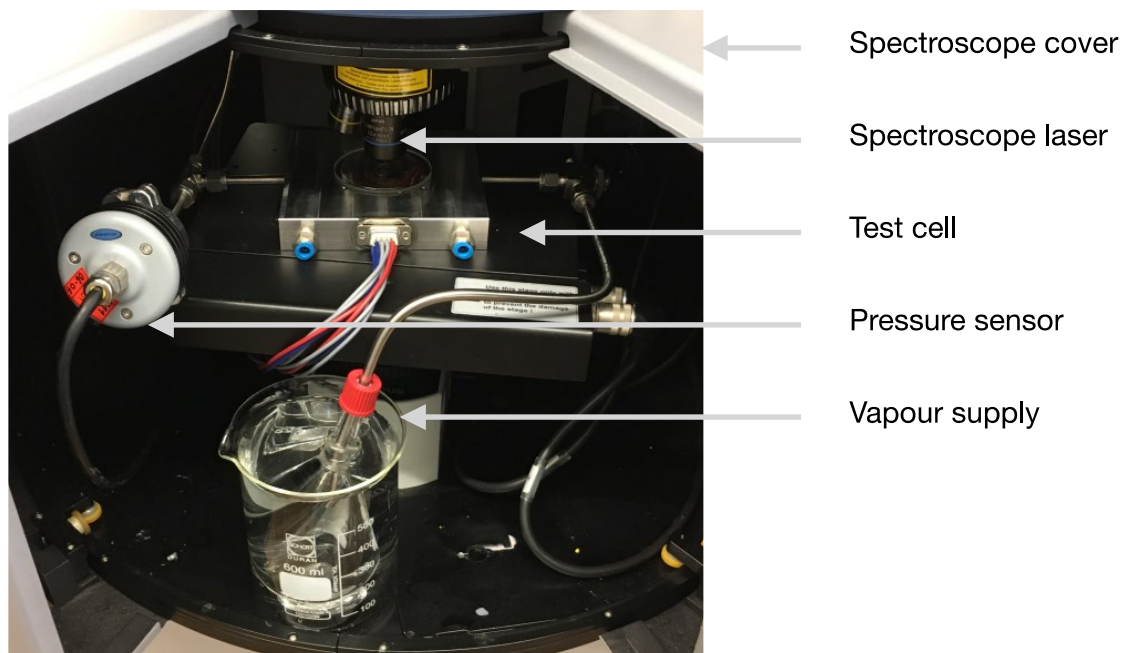

Figure 3: Picture of the test setup.

Raman spectroscopy can be used to measure the ratio of water to sodium hydroxide (concentration) in the solution at different depths in the film (Figure 2b). A drop of sorbent solution was placed on a Peltier element for heating (desorption) and cooling (absorption). The cell was covered with glass for laser transparency and connected to a vacuum pump and vapor supply for vapor pressure control (vapor atmosphere). In this way, the resulting gradient in absorption and desorption can be measured under realistic operating conditions.

It was expected that the result of this study would provide an understanding of the limitations of mass uptake/release and transport in the absorbent film. The formation of a concentration gradient was thought to be indicative of mass transport limitations within the sorbent (mass diffusion of water into sodium hydroxide) rather than surface barriers on the sorbent.

1.5 Neutron imaging absorption visualization cell

An optical study was conducted to visualize the absorption of water vapor on sodium hydroxide. It was expected that prospects for absorption enhancement could be found. For this work, the SINQ neutron imaging facility at PSI (Paul Scherrer Institute) was used. Neutrons are particularly sensitive to hydrogen, making the presence of water in a solution well visible. To enhance the contrast between the absorbed water (H_2O) and the absorbing aqueous sodium hydroxide solution (NaOH + H_2O), a solution of sodium deuteroxide (NaOD) in deuterium oxide (D2O) was used. Deuterium, or heavy hydrogen with a neutron, is transparent to the neutron beam, while normal hydrogen without a neutron is not. A cell was built as shown in Figure 4. Again, it was possible to control the atmosphere of pure water vapor in the cell, while droplets of aqueous sodium deuteroxide were supplied from the central tube. Figure 5 shows the principal visualization and a neutron image of the cell during the test.
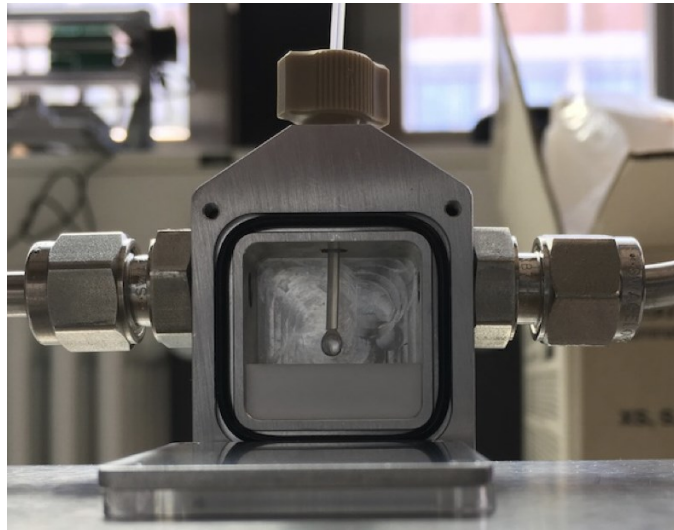
Figure 4: Picture of the uncovered test cell, showing a droplet of absorbent at the end of the supply tube.
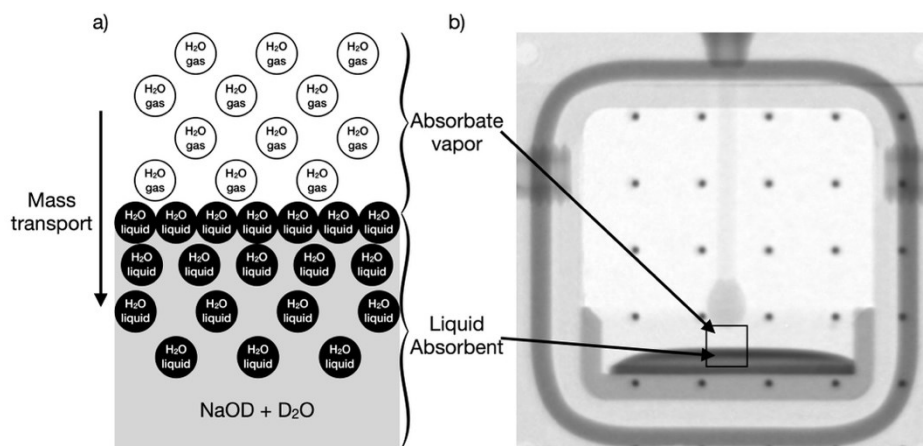

Figure 5: a) Illustration of the visualization of absorbate mass transport. The gaseous absorbate is transparent and becomes visible (black) when liquified on the absorbent surface and transports into the absorbent film. b) Neutron image of the cell showing the chamber vaper volume (H_2O gas), droplet supply and absorbent film (NaOD + D_2O). The black dots are for orientation purpose only, originating from an afore-placed aluminum sheet containing highly neutron scattering inlays.

1.6   Laboratory scale absorption heat and mass exchanger test rig

Based on the understanding of the absorption process, that the temperature gain is directly related to the concentration and the energy density to the concentration difference, and the results of the tests performed with the previously described setups, it was found that an approach using a commercially available standard spiral filled tube may be promising. In this heat and mass exchange idea, the absorbent flows from top to bottom in the spiral fin and the heat transfer fluid flows from bottom to top in countercurrent through the inner tube. This design provides a long exposure time for absorbent uptake. To test the idea, a laboratory-scale test rig was built to accommodate a desorber/absorber and a condenser/evaporator spiral fin tube. Figure 6 shows an image of the setup.
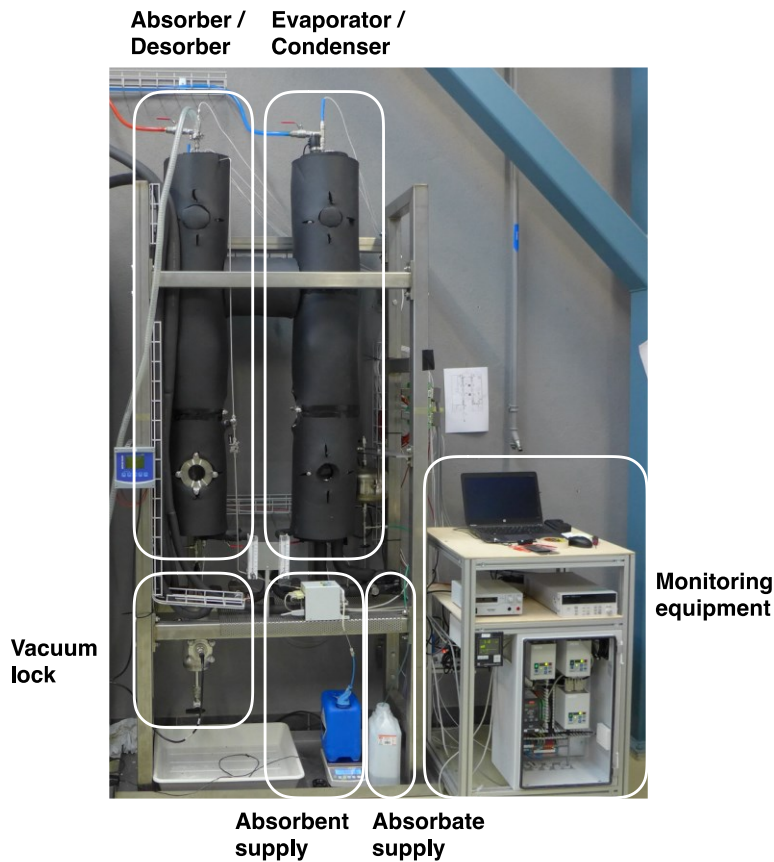
Figure 6: Picture of the lab scale spiral finned tube heat and mass exchanger test bench.

1.7 Single-family home scale absorption heat storage demonstrator

Based on the successful testing of the novel spiral fin heat and mass exchanger on a small (single tube) scale, an upscaling was conducted. This consisted of 2 x 100 tubes fed equally with absorbent or absorbate and heat transfer fluid. Figure 7 shows the demonstration system. The setup consists of the heat and mass exchange unit (steel vessel center/right) and the storage vessels (left/back). Absorbent and absorbate were pumped back and forth between the storage vessels and the heat and mass exchanger. The system was controlled and monitored using LabVIEW®, and cooling and heating machines were used to mimic the heat source and sink in the desorption and absorption. The spiral fin tubes were bundled into sets of 10 tubes and installed in the heat and mass exchanger housing as shown in the lower left image in Figure 7, and the individual tubes were fed with absorbent and absorbate as shown in the lower right image. The main challenge was to ensure equal distribution of all the liquids.
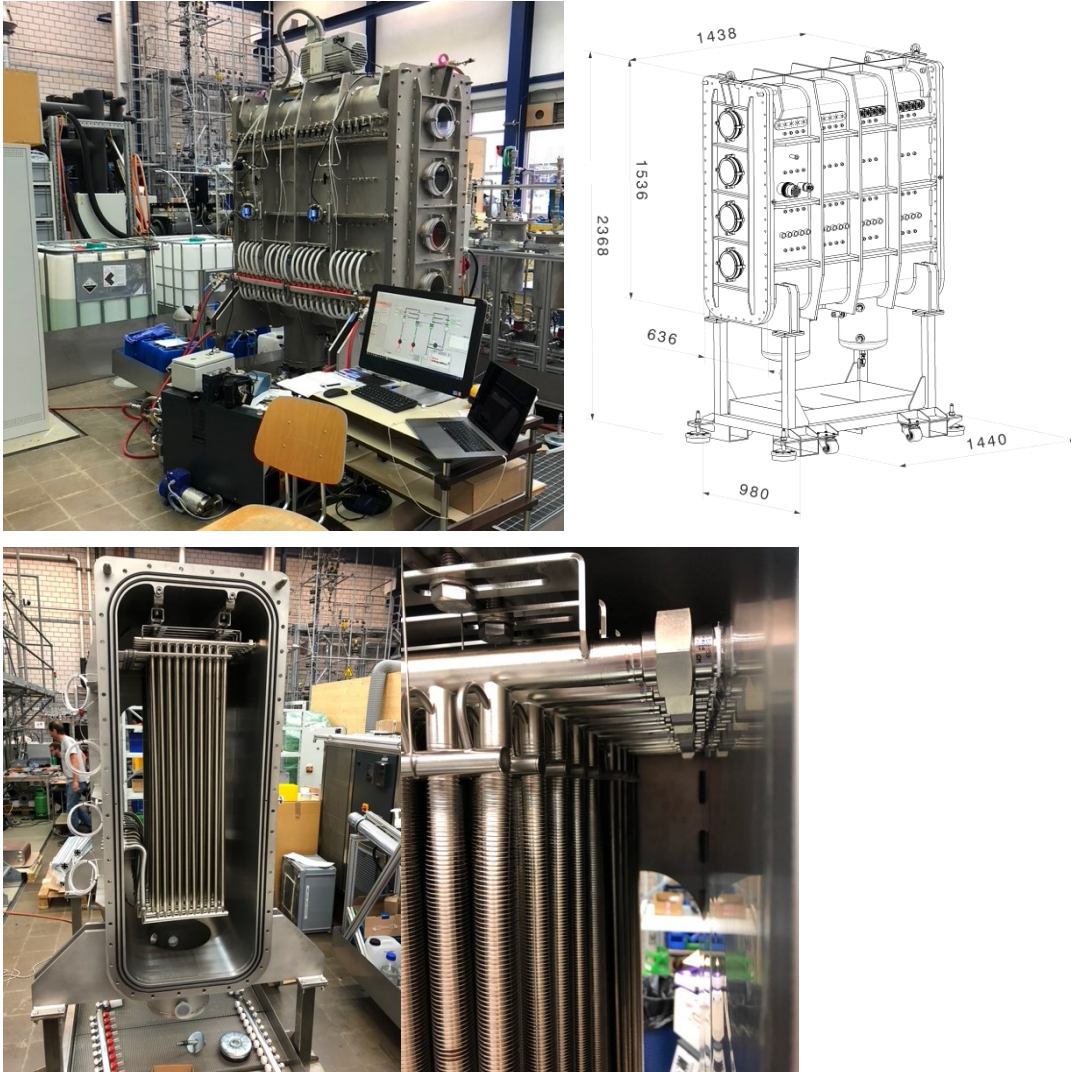
Figure 7: Left top: Image of the upscaled HMX installed in the HSLU lab. On the left back side, the aqueous NaOH tanks are visible. Right top: Drawing of the upscaled HMX with dimensions in mm. Left bottom: Image of the installed spiral finned tube elements. Right bottom: Image of the individual distribution nozzles.

2 Procedures and methodology

2.1 Raman spectroscopy mass transport analysis

To measure the water content in aqueous sodium hydroxide solution, a compound selective method was needed that was compatible with the corrosive medium and could provide the required resolution. Since water and aqueous sodium hydroxide are transparent, a Raman spectroscopy (visible light based) approach was pursued. Raman spectroscopy provides structural fingerprints from which molecules can be identified and traces can be assembled to create a 3D image of the material under study. In this work, time-resolved measurements of sodium hydroxide concentrations at different film depths were obtained in the process of absorption and desorption. The time resolution was in minutes and the spatial resolution was in the 10 µm range. A SENTERRA® spectrometer (532 nm) was used with a custom designed sorption analysis cell.

Calibration measurements were done, based on well-defined concentrations, and a calibration curve derived, see figure 8.
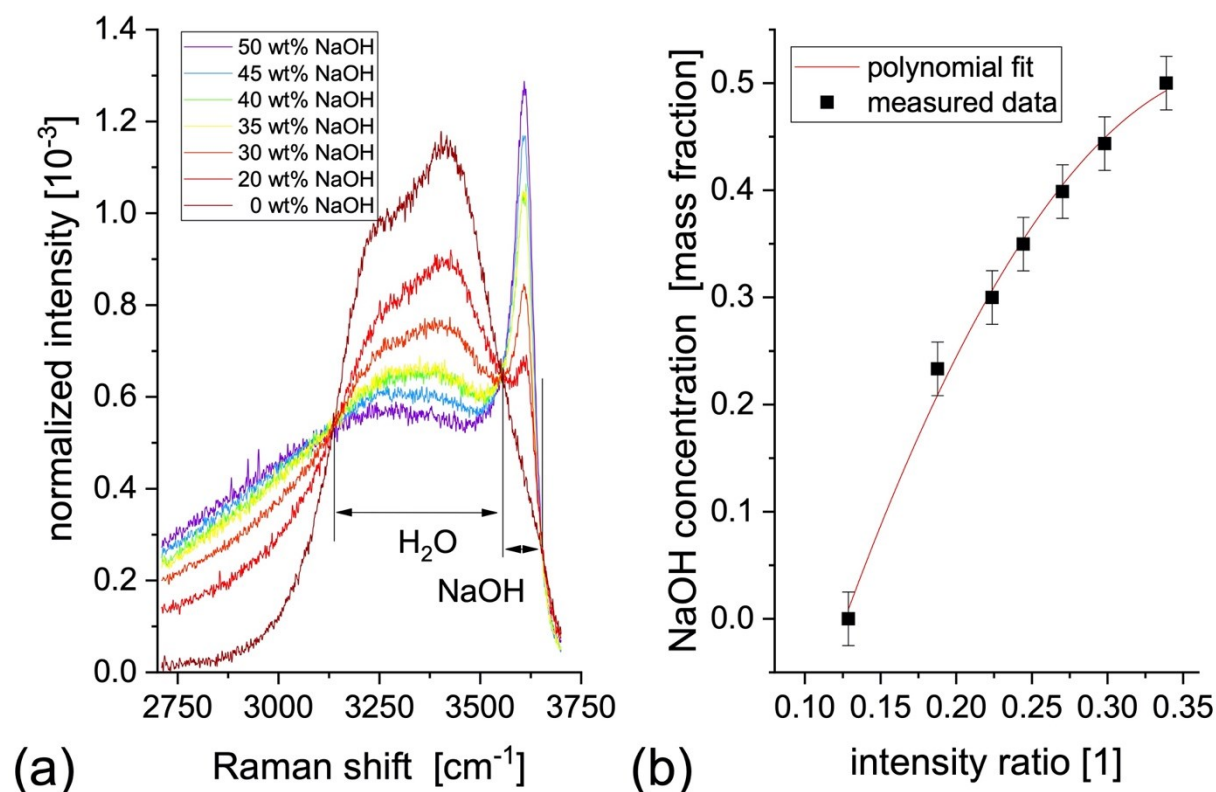
Figure 8: a) Total intensity normalized Raman spectra of aqueous sodium hydroxide solutions at different concentrations; the lines indicate the isosbestic points that define the integration limits for quantification. b) Calibration curve to determine the sodium hydroxide concentration, derived from the intensity ratio of the two integration areas in (a).

During the measurement, a drop of aqueous sodium hydroxide was placed on the Peltier element and lightly smeared to form a thin film (approximately 200 µm). All non-condensing gases were removed by applying a vacuum to create an absorbate vapor atmosphere. By changing the temperature of the drop, the thermodynamic equilibrium of the drop with respect to the vapor pressure changed and water

was absorbed or desorbed. The position of the gas-liquid interface changed with the absorption and desorption due to the uptake and release of water, as shown in Figure 2b. For this reason, measurements were made at a defined distance from the focal point to the bottom of the film (the sample holder). A measurement sequence, which included a temperature change from high to low for absorption and from low to high for desorption, consisted of 49 Raman spectral measurements with a time resolution of 10 s. A complete evaluation consisted of six sequences with a focal point change of 50 µm depth per sequence.

2.2   Neutron imaging absorption visualization

In this study, a possibilities of enhancing mass transport from the absorbing surface to the bulk was investigated. An initial idea of droplet impingement and suspension led to the prospect of mixing by buoyancy movement.

The neutron is a unique probe in nondestructive materials science because it interacts weakly with many high-density materials. Hydrogen is one of the most powerful neutron scatterers. For this reason, the imaging technique is very sensitive to water. In addition, neutrons are isotope sensitive. There is a large difference between the hydrogen isotopes 1H and 2H (D, deuterium). This characteristic is used in the study to improve the visible separation between isotopically enriched absorbent (NaOD in D_2O) and the absorbate (H_2O).

The temporal and spatial resolution of the images are mutually limited by the neutron flux. One is optimized at the expense of the other. In this study, exposure times of 0.1 s and 1.0 s are used with a resolution of 44 µm. The test object is positioned close to the scintillator screen to reduce the amount of penumbra blurring.

An aluminum test cell was constructed as shown in Figure 4. Aluminum is largely transparent to neutrons and can withstand the applied pressure difference between vapor and atmosphere (about 1 bar). All gases except water vapor are removed from the cell. To prevent contact with the absorber, a polytetrafluoroethylene (PTFE) tray is inserted into the cell. Like aluminum, PTFE is largely transparent, has a relatively low attenuation coefficient, and does not contain hydrogen. Samples are placed on a stainless-steel plate at the bottom of the tray. A thin PTFE tube is inserted from the top of the cell for sample delivery. The cell is connected to a water (H_2O) vapor source, a vacuum pump, and a pressure sensor. The supply of absorbent is controlled by a peristaltic pump. Figure 9 shows the cell installed in the beam line.

Observation of absorption and convection is performed under two different conditions: droplet impingement and droplet suspension. The tests were performed at a water vapor pressure of 2.33 kPa, corresponding to an evaporation temperature of 20 °C, and an absorbent concentration of 40 wt% NaOD in D_2O.

Figure 9: Picture of the installed cell in the neutron beam line.

2.3 Laboratory scale absorption heat and mass exchanger

A small-scale absorption heat and mass exchanger test bench was built to investigate the novel idea of a spiral finned tube heat and mass exchanger both in the absorption and the desorption processes.

The heat and mass exchanger idea basis on a standard spiral fin tube heat exchanger arranged vertically. In this way, an open channel with low slope is provided by the continuous screw type form of the fin spiraling downwards around the central tube, as illustrated in figure 10.
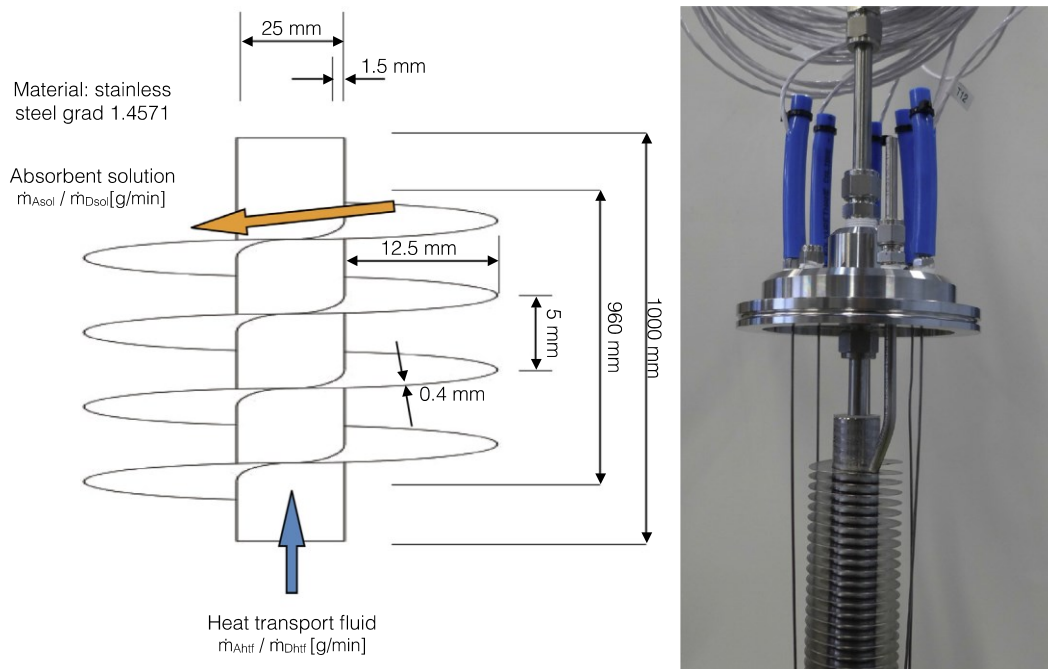
Figure 10: Left: Illustration of the spiral fin tube heat exchanger with absorbent and heat transfer fluid flow. Right: Picture of the heat and mass exchanger with absorbent supply tube and temperature sensors installed.

Absorbent solution applied to the spiral fin channel flows slowly down the tube along the fin by gravity, allowing extended time for absorption or desorption and heat exchange with the heat transfer fluid in the tube, which flows in a countercurrent direction from bottom to top. A steady temperature and concentration gradient is created across the fin in a continuous flow of absorbent solution film. Good wetting of the heat and mass exchanger is achieved by strict channeling.

The test setup was constructed as shown in Figure 6 and illustrated in Figure 11. The heat transfer fluid temperatures were controlled by two heating/cooling machines and the flows were controlled by two precision gear pumps. The absorbent was pumped by a peristaltic pump from the blue canister placed on a mass scale. The absorbate was circulated by a gear pump. All temperatures were recorded using Labview®. Installed vacuum locks allowed removal of absorbent and absorbate without interfering with the operating process. Absorbate concentration was determined by density and temperature measurement.

Spiral finned tubes of various dimensions and materials were measured under application specific operating conditions (temperatures) in respect to output temperature, power and final absorbent concentration (energy density).
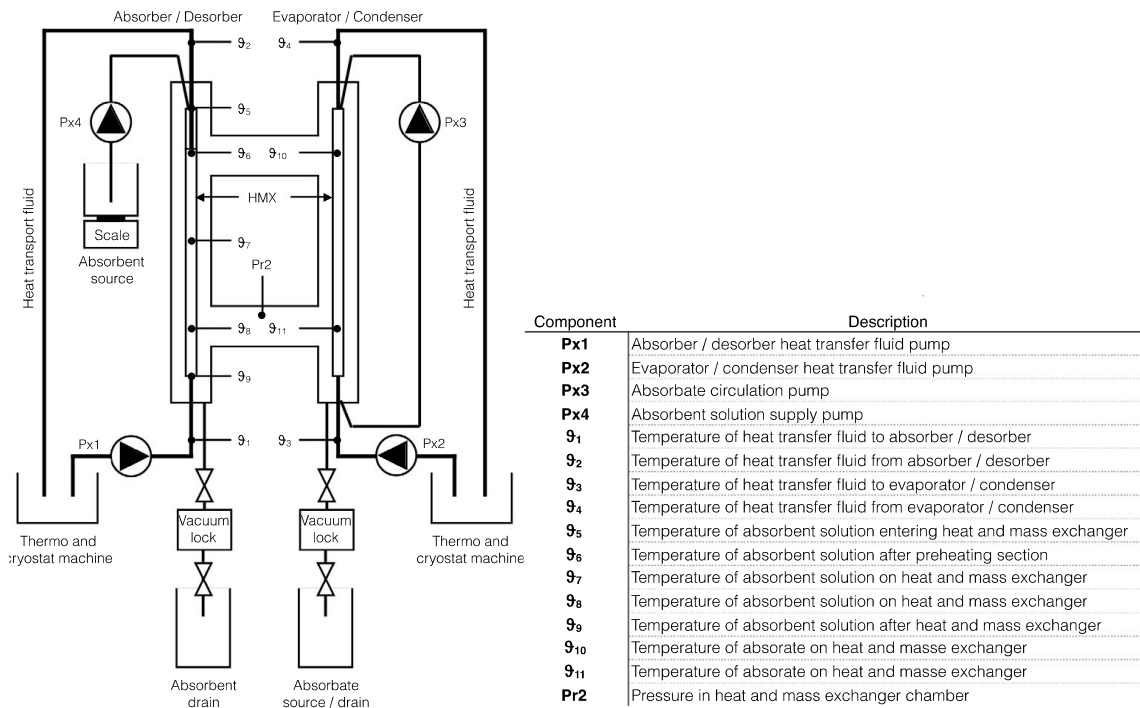

Component	Description
Px1	Absorber / desorber heat transfer fluid pump
Px2	Evaporator / condenser heat transfer fluid pump
Px3	Absorbate circulation pump
Px4	Absorbent solution supply pump
ϑ_1	Temperature of heat transfer fluid to absorber / desorber
ϑ_2	Temperature of heat transfer fluid from absorber / desorber
ϑ_3	Temperature of heat transfer fluid to evaporator / condenser
ϑ_4	Temperature of heat transfer fluid from evaporator / condenser
ϑ_5	Temperature of absorbent solution entering heat and mass exchanger
ϑ_6	Temperature of absorbent solution after preheating section
ϑ_7	Temperature of absorbent solution on heat and mass exchanger
ϑ_8	Temperature of absorbent solution on heat and mass exchanger
ϑ_9	Temperature of absorbent solution after heat and mass exchanger
ϑ_{10}	Temperature of absorate on heat and masse exchanger
ϑ_{11}	Temperature of absorate on heat and masse exchanger
Pr2	Pressure in heat and mass exchanger chamber

Figure11. Schematics of the heat and mass exchanger with component placement

2.4　Single-family home scale absorption heat storage system

Based on the results of the small-scale absorption test bench, a spiral finned tube was chosen for the upscaling. The upscaled system was designed to meet the power requirements of a single-family home (4-6kW) and to operate with a comparably large amount of aqueous sodium hydroxide (1200kg). The system consists of two main parts, the heat and mass exchanger and the absorbent and absorbate storage tanks.

The heat and mass exchanger is designed as an airtight low pressure vessel because the system operates in a vapor atmosphere where the pressure is dependent on the evaporator/condenser temperature. Inside the vessel are two heat and mass exchange elements that act as an absorber/desorber and an evaporator/condenser. These consist of 10 spiral fin tube elements with 10 spiral fin tubes of 1m length each (200 tubes in total). Inside the tube the heat transfer fluid flows from bottom to top, outside the tube the absorbent or absorbate flows from top to bottom along the spiral fin in counterflow to the heat transfer fluid. A key criterion for good operation of the heat and mass exchange unit is the uniform distribution of both the heat transfer fluids and the absorbent and absorbate.

The test setup consists of the heat and mass exchanger unit, shown as HMX in the diagram in Figure 12, connected to two heating and cooling machines (Regloplas®). Gear pumps (P1-P3) are used to pump absorbent and absorbate to and from the heat and mass exchanger and the pallet-sized plastic tanks. Flowmeters are used to measure the absorbent and absorbate flow. The heat transfer fluid outlet temperatures of each spiral fin tube element (10 tubes) and the total heat transfer fluid inlet and outlet temperatures are monitored.
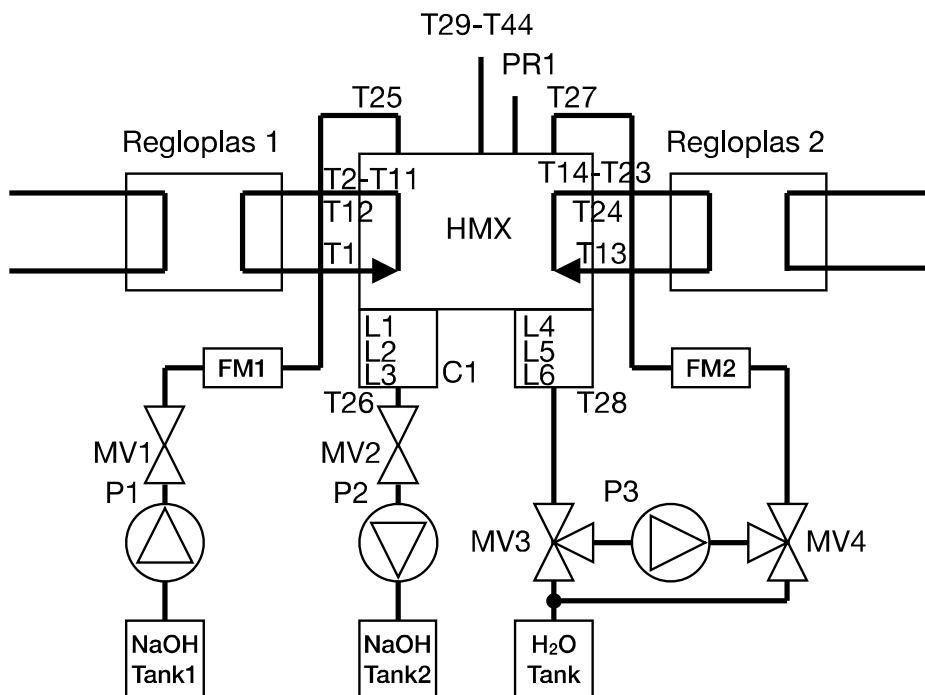

Figure 12: Schematics of the single-family scale absorption heat storage system.

2.5 Simulation of the sorption heat storage in a building

The integration of a sorption heat storage system into a building has been simulated in Trnsys®. The simulation includes solar collectors, 3 water tanks (domestic hot water, space heating, buffer tank), NaOH sorption tank, geothermal heat exchanger, auxiliary heating (electric) and thermal load for space heating (floor heating system) and domestic hot water. Figure 13 shows a schematic of the simulated system.
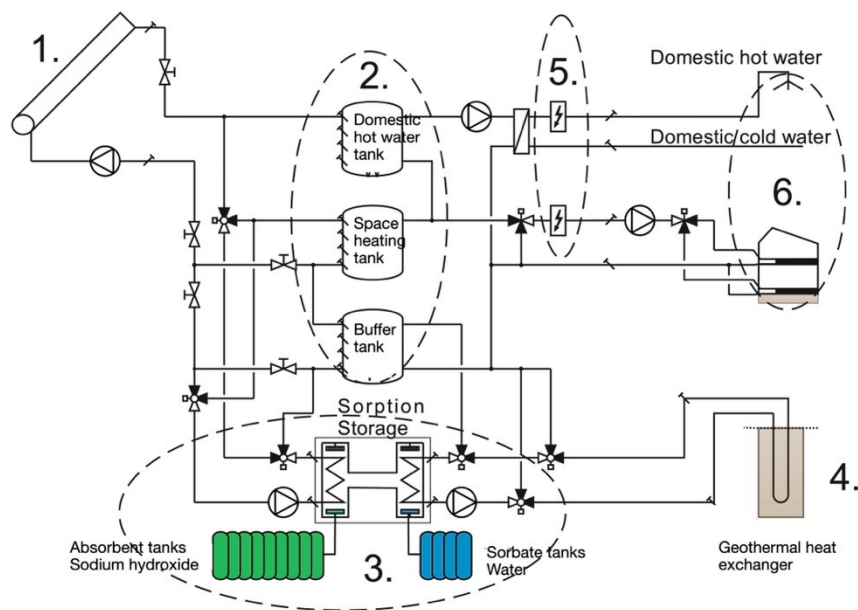

Figure 13: Schematic representation of the simulated system.

The simulation work was based on the initial results of the single tube laboratory scale heat and mass exchanger (gray box). Since these tests were performed at non-specific application temperatures, linear extrapolation was necessary. The simulation work is configured with solar thermal collectors as the high temperature heat source, in a purely thermal building energy system with a geothermal heat exchanger as the low temperature heat source and sink. A parametric analysis was carried out. The objective of the study was to determine the component sizing and system configuration for different building types and climates.

The study simulates four different buildings, two single-family homes and two multi-family homes, see Table 1 and Figure 14.

Table 1: List of the simulated buildings.

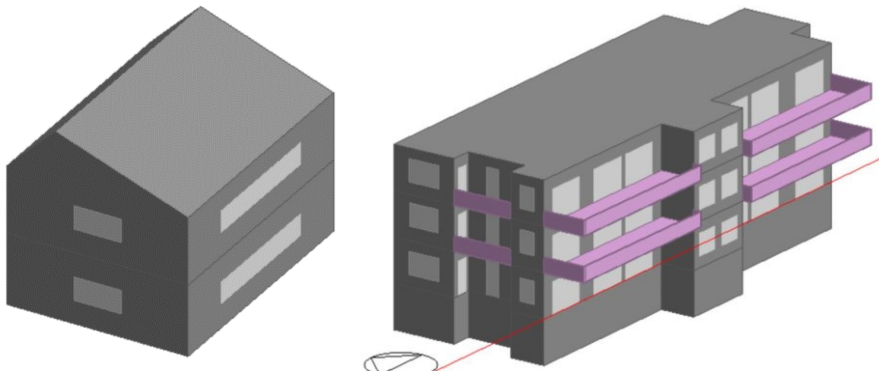|	Living space	Occupants	Heating energy demand	Roof area	Collector area
SFH45	140 m²	4	45kWh/(m²·a)	57m²	Max. 50m²
SFH100	140 m²	4	100kWh/(m²·a)	57m²	Max. 50m²
MFH30	1205 m²	18	30kWh/(m²·a)	382m²	Max. 340m²
MFH90	1169 m²	18	90kWh/(m²·a)	382m²	Max. 340m²

Figure 14: Left) Single-family home, Right) multi-family home.

The buildings vary in living area, number of occupants and thermal insulation. The number in the building abbreviation refers to the heating load per square meter and year. In each case, the collector surface is oriented toward the south with an inclination of 50° (90° ≙ vertical) and is limited by the roof surface. The building internal loads are taken from the IEA SHC Task 44 and the climate profiles of the selected climate locations (Table 2) were created with Meteonorm 7.1.8. The heating load profiles sourced from EnergyPlus were imported into the TRNSYS simulation and the domestic hot water profile was taken from IEA SHC Task 26.

Table 2: Applied climatical conditions.

	Zurich	Helsinki	Harbin
Koordinaten	47.4°N, 8.5°O	60.2°N, 24.9°O	45.8°N, 126.5°O
Durchschnittliche Tagestemperaturen Januar	-1°C bis 4°C	-8°C bis -3°C	-13°C bis -24°C
Durchschnittliche Tagestemperaturen Juli	14°C bis 24°C	13°C bis 21°C	18°C bis 28°C
Kaltwassertemperatur	10.0°C	7.0°C	6.5°C

The number of sorbent and sorbate storage tanks depends on the resulting demand of the parameter selection. This means that the minimum quantity of sodium hydroxide during loading or unloading limits the storage volume.

The solar collectors supply the buffer tanks (serial flow, starting with the domestic hot water tant to the space heating tank and finally the buffer tank). This heat is first used to meet the energy needs of the building (direct feed), then the NaOH storage tank is charged. In case of overtemperature in the buffers and charged sorption storage, heat is dissipated to the borehole heat exchangers.

To charge the NaOH storage tank (charging), heat is taken from the buffer tanks; when discharging, heat is fed back into the buffer tanks. The waste heat generated during charging is dissipated in the borehole heat exchanger, while the ambient heat required for discharging is taken from the borehole heat exchanger.

The domestic hot water is produced by a hot water station (heat exchanger), which receives the heating water from the DHW buffer tank. In case of insufficient temperature, the domestic hot water is further heated by the additional electric heating.

The heating of the building is supplied by the heating buffer (SH). In this case, too, if the supply temperature is insufficient, the water is heated electrically by an auxiliary heater.

The cost calculations were performed based on the SFOE final report OPTSAIS [60]. As often as possible, costs and calculation methods were taken from this report or adapted. In general a fixed cost contribution and a contribution per unit was used. The cost of caustic soda is the same as the cost of filling during the COMTES project [61]. The cost of the PP tanks is based on a calculation by Kingspan, partner in the COMTES project and producer of PP tanks itself. It is assumed that 2m³ tanks with catch basins can be used. In addition, the maximum number of tanks for the caustic is calculated by taking the required volume [m³] of diluted caustic and desorbed water as a benchmark. Additionally, indirect costs, space requirements, were included. Table 3 shows the costs taken.

Table 3: Factors for the calculation of specific solar energy costs.

Solar collectors [60]	$300 \cdot A_{sol}$ + CHF 200
Solar collector installation [60]	$260 \cdot A_{sol}$ + CHF 9000
Buffer tank [62]	1379.75 CHF $\cdot$ m³
Geothermal heat exchanger [63,64]	CHF $70 \cdot$ m
Geothermal heat exchanger installation [63,64]	CHF $3000 \cdot$ #Pipes
Sorption heat and mass exchanger	CHF $1200 \cdot$ kW
Sodium hydroxide	CHF $500 \cdot$ m³
PP-Tank	CHF $200 \cdot$ m³
Return on capital (i)	1%
Payback period (n)	GHX: 50 Jahre, Kollektor & Speicher: 20 Jahre
Annuity [60]	$((1+i)^n \cdot i)/((1+i)^n - 1)$ $\qquad$ (18)
Maintenance factor β	Geothermal heat exchanger: 0.5%, Collectors and storage: 2%
Cellar rent [65]	CHF $100 \cdot$ m²

2.6 Application specific static testing temperatures

For this project, a set of realistic temperatures for static testing has been developed based on the temperatures defined in the European heat pump testing standards. In the past it has been recognized that the performance of the sorption heat storage system in terms of outlet temperature, output power and energy density is highly dependent on the operating temperatures. Figure 15 shows the required test temperatures for the closed transported process, and Table 3 shows the defined values.
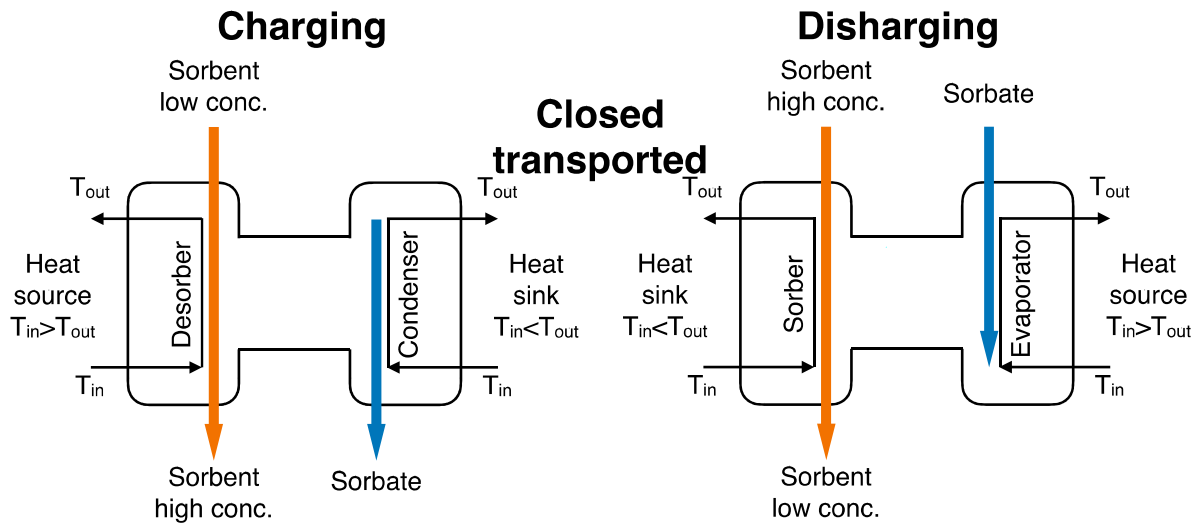
Figure 15: Illustration of the closed transported processes in charging and discharging. Indicated are the relevant heat source and sink temperatures.

Table 3: Temperature guideline for uniform sorption thermal storage testing for space heating in buildings.

Process	Input Temperature (Vapor Pressure *)	Output Temperature
Desorption	95 °C (3.0 kPa)	92 °C
Condensation	30 °C	35 °C
Evaporation	10 °C (0.87 kPa)	7 °C
Sorption	30 °C	35 °C

* Vapor pressure is relevant only for open systems.

Based on this testing guideline it is possible to evaluate how well a sorption heat storage system works, and comparison with other systems is possible.

2.7   Heat and mass exchanger performance mapping

Work has been done on the performance evaluation applicable to the heat and mass exchanger (system) level. At the material scale, the theoretical maximum outlet temperature and energy density are related to the equilibrium condition. Any deviation from this is due to heat and mass transport limitations. At the practical scale, there is an additional limitation based on the nonlinearity of the temperature gain to the heat released from the absorbent. This is due to the dependence of the temperature gain on the absorbent charge state (concentration) and the relative increase in absorber uptake as the charge state decreases. As the absorbent concentration decreases, the water uptake required for the concentration decline, increases. The result of these phenomena is that the temperature-dependent heat release during discharge is equal to the linear heat capacity of the heat transfer fluid at only one point. Therefore, both maximum temperature gain and maximum energy density cannot be achieved simultaneously. Figure 16 shows the deviation from material equilibrium as a function of the ratio of heat transfer fluid to absorbing fluid flow (FR).
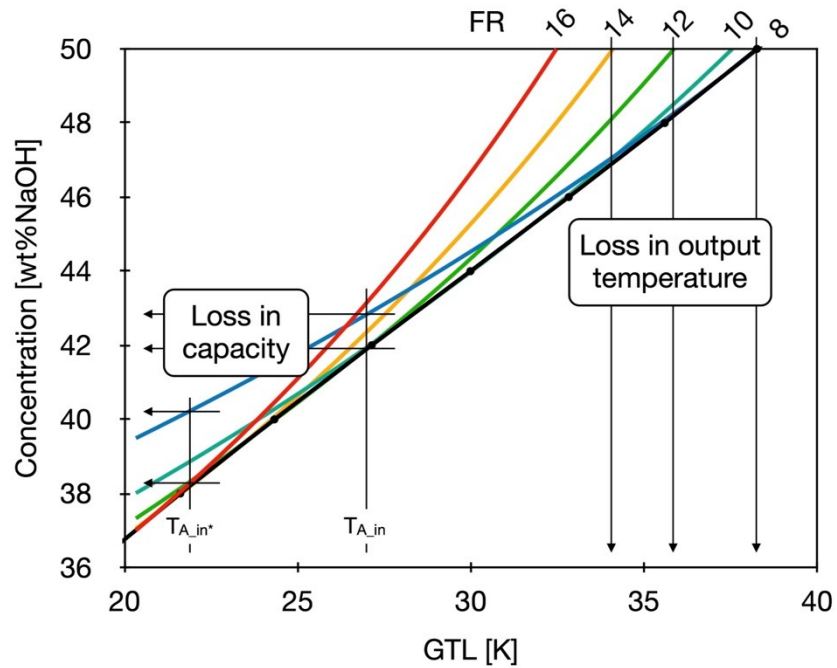
Figure 16: Diagram showing concentration vs gross temperature lift (GTL) at an evaporating temperature of 5°C. Included are flow ratio (FR) curves of 8 to 16. Deviation from the equilibrium curve indicates temperature decline and storage capacity loss.

This approach to performance evaluation (mapping) provides the basis for a clear assessment of the functionality of the entire heat and mass exchanger. The deviation of the flow ratio curve from equilibrium visualizes the unavoidable heat capacity mismatch. Operating results, heat transfer fluid outlet temperature at 50wt% concentration and final concentration at heat transfer fluid inlet temperature, are mapped (dots placed) on the graph indicating the deviation from the flow ratio curve (practical maximum).

3 Results and discussion

3.1 Raman spectroscopy mass transport analysis results

A series of measurements on the time-resolved concentration changes during absorption and desorption at varying focal points of the sorbent solution film were derived. Figure 17 shows an example of a measurement sequence.
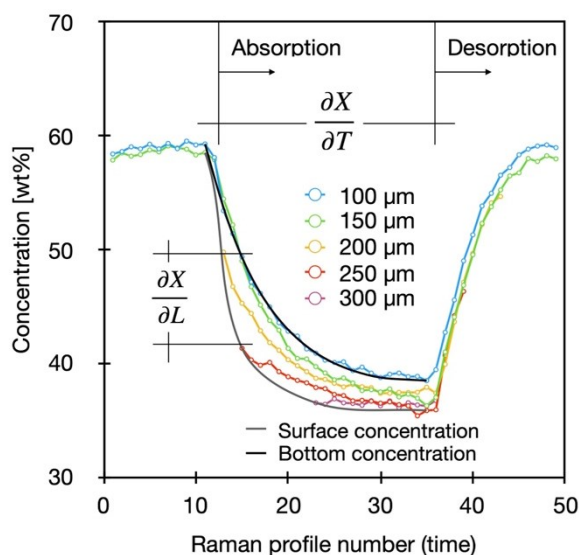

Figure 17: Resulting concentration change on an absorbent firm measured operando during water absorption and desorption at a temperature of 35°C and 55°C, respectively, and a constant vapour pressure of 8.7mbar

The purpose of this study was to determine whether the uptake of water vapor on aqueous sodium hydroxide is controlled by surface phenomena or by mass diffusion in the film. We reasoned that if a concentration gradient was found, it would indicate that diffusion was the dominant resistance.

From the measurement results, it was shown that a concentration gradient is established and that it degrades over time to a lower concentration equilibrium in absorption and a corresponding higher concentration steady state in desorption. Thus, mass diffusion in the film was found to be the dominant resistance under the measured application-realistic conditions. The exponential, time dependent concentration decrease in absorption and concentration increase in desorption was further strong indications in support of a diffusion controlled process.

It was found that reference and measured values are closely fitting, as show in figure 18.
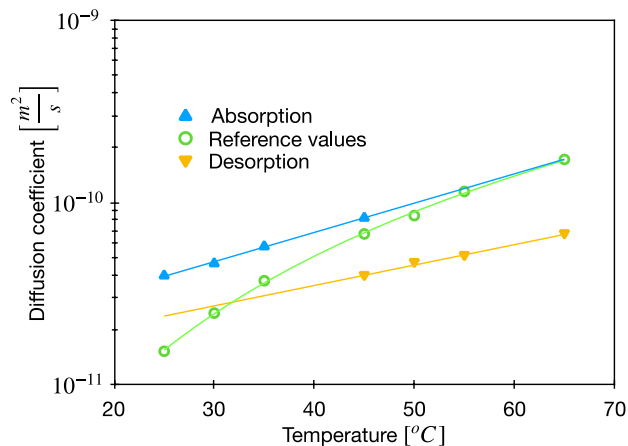
Figure 18: The diffusion coefficient of water in aqueous sodium hydroxide at various temperatures.

Since the uptake and release of water on sodium hydroxide is limited by the mass transport of water in aqueous sodium hydroxide, methods to enhance mass transport were of interest.

3.2 Neutron imaging absorption visualization results

The goal of the neutron imaging study was to investigate the potential for mass transport enhancement of water in aqueous sodium hydroxide solution. Observation of absorption and convection was performed under two different conditions: droplet impingement and droplet suspension.

Figures 19 and 20 show the results of the drop impact tests. Droplet D1 impinged directly on the steel plate without an absorbent film and showed rapid distribution with immediate vapor absorption, forming a film 0.26 mm high. When the second droplet, D2, impinged, the film of dilute absorbent was pushed aside, forming a pool of concentrated absorbent within a ring of dilute absorbent. The pattern formed showed that there was little mixing of the dilute and concentrated absorbents. It appears that the drop broke through the existing film, spread by impact on the steel, and washed the dilute absorbent to the side. The third drop, D3, confirmed this tendency by further pushing the dilute absorbent from the center outward. As the film height increased in D4, a different pattern began to develop. As fresh absorbent droplets fell through the surface of the absorbent film and dispersed upon impact with the stainless steel, the concentrated absorbent moved underneath the diluted absorbent. As the film height increased and the ratio of film height to droplet diameter decreased, the lateral movement of the dilute absorbent decreased and the impact and spreading process evolved more into a process of pearling through the surface area of the semi-dilute absorbent and deposition of the fresh absorbent underneath. Comparing D4 to D6, there is spreading of the concentrated absorbent under the dilute absorbent.

The final image sequence from this series, shown in Figure 21, does not follow the pre- and post-drop pattern, but provides a time sequence of images including a drop impact. The images were taken with an exposure time of 1 s and show the movement and development of the absorbing film. The process seen in D4 to D6 was further confirmed, with concentrated absorbent spreading along the sheet and diluted absorbent floating over it. A new pattern developed from time T = 0s to T = 1s. By floating over the concentrated absorbent, the dilute absorbent broke away from the sides, exposing the concentrated absorbent directly to the water vapor. The final drop was added at T = 4s. At this stage, no spreading of the absorbent was observed, only an increase in film height and thus a slight elevation of the dilute film above the concentrated absorbent (film height increase from 1.36mm to 1.45mm). Further images showed that, interestingly, the concentrated absorbent exposed to the side was not covered, but the height of the concentrated absorbent continuously decreased, and the height of the diluted absorbent film increased.
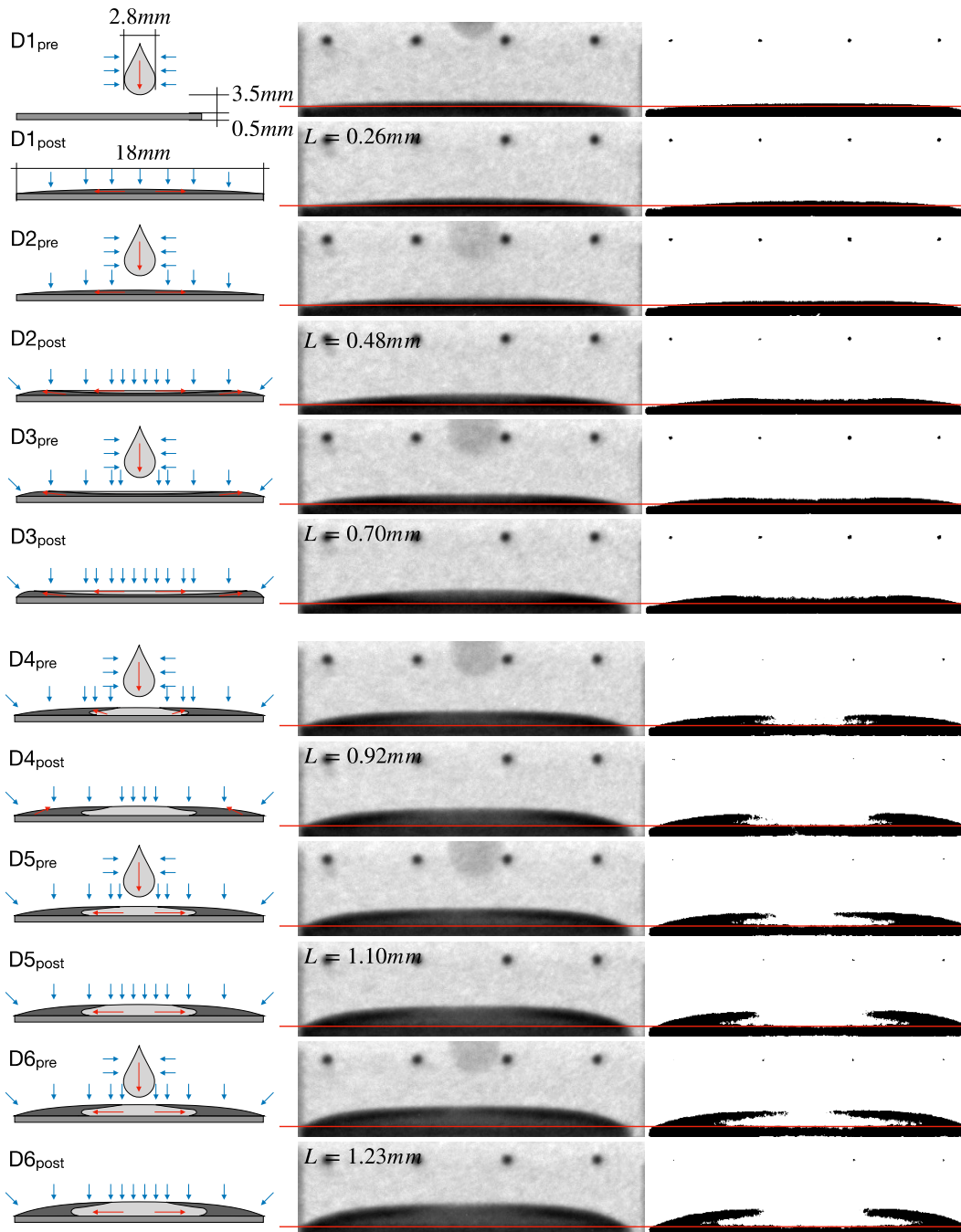
Figure 19: Droplet impingement images taken at an exposure time of 0.1s. Each process step consists of a sketch, a regular image, and a contrast-enhanced image highlighting the dilute absorbent (black). The red line indicates the separation between the stainless-steel plate and the absorbent. Dark areas above the red line are areas of dilute absorbent containing absorbed H2O. "Pre" indicates just before impingement and "post" indicates just after impingement. The time between pre and post was 0.2 s. The time between droplets was approximately 10 s.
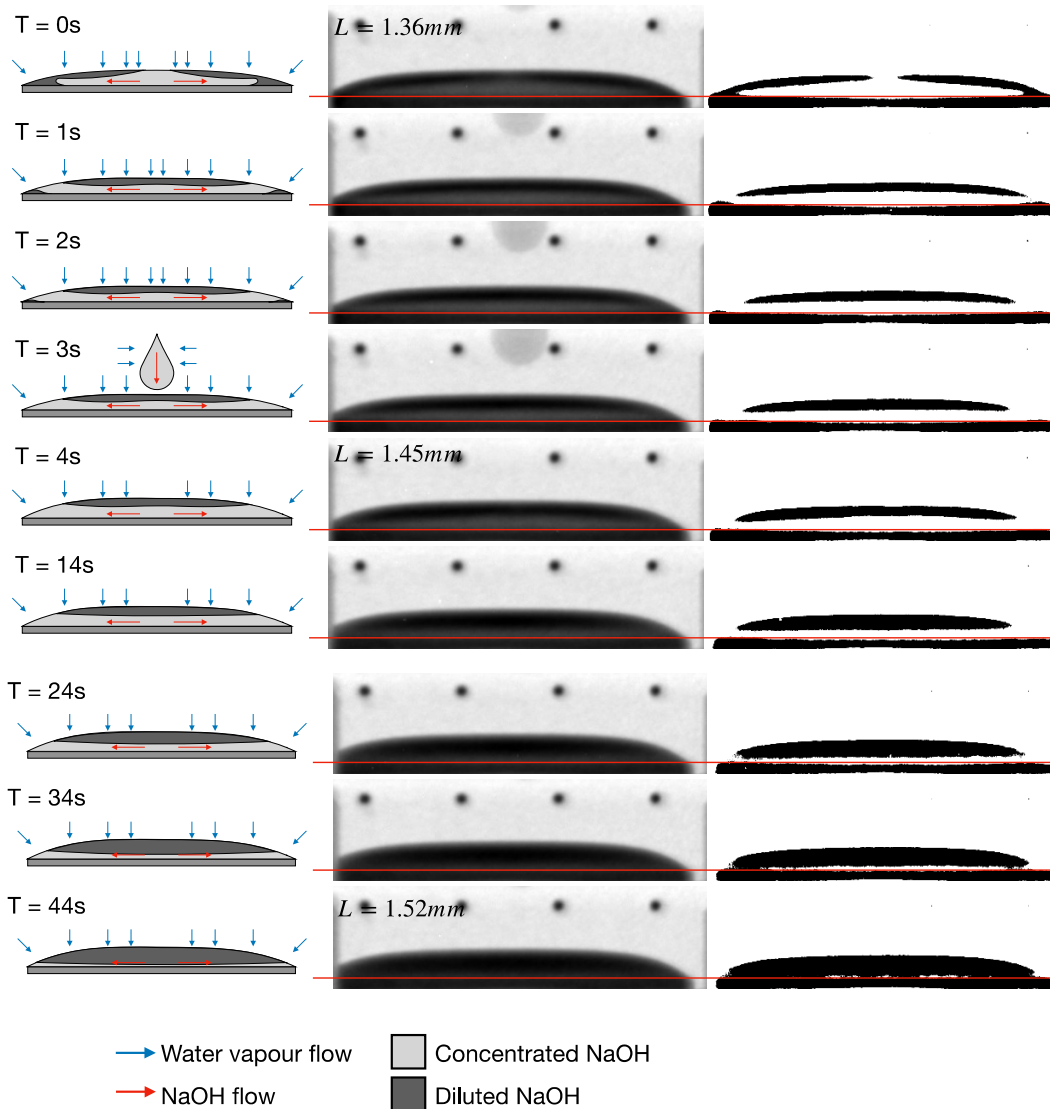
T = 0s $L = 1.36mm$

T = 1s

T = 2s

T = 3s

T = 4s $L = 1.45mm$

T = 14s

T = 24s

T = 34s

T = 44s $L = 1.52mm$

→ Water vapour flow   ☐ Concentrated NaOH

→ NaOH flow   ■ Diluted NaOH

Figure 20: Images of the droplet impingement and sorption process taken at an exposure time of 1 s. T = x is the elapsed time.

In the droplet suspension test, a dilute droplet was suspended from a stainless-steel wire mesh and a fresh absorbent droplet was supplied from a tube above the absorbent, as in the previous droplet impact tests. Figure 21 shows the results of this sequence, again with an illustration, a normal image, and a contrast-enhanced image. The images are taken with an exposure time of 0.1 s. Image T = 0 shows the initial setting with the dark droplet attached to the fabric. The fresh droplet before falling can be seen in light gray just above the diluted droplet. At time T = 0.2s, the fresh droplet has fallen and collided with the metal screen and the dilute droplet. Interestingly, just after the first impact, the concentrated, heavy absorbent was seen to sink to the bottom of the droplet. It appears that there was virtually no mixing of the dilute and concentrated sorbent. From time T = 0.4s, a separation between dilute and concentrated sorbent developed, and by time T = 2.4s, the combined droplets had separated into a concentrated solution at the bottom and a dilute region at the top. It was shown that a fast and strong separation occurs. The droplet suspension has the advantage that the concentrated sorbent is strongly exposed to the absorbate at the bottom of the droplet.
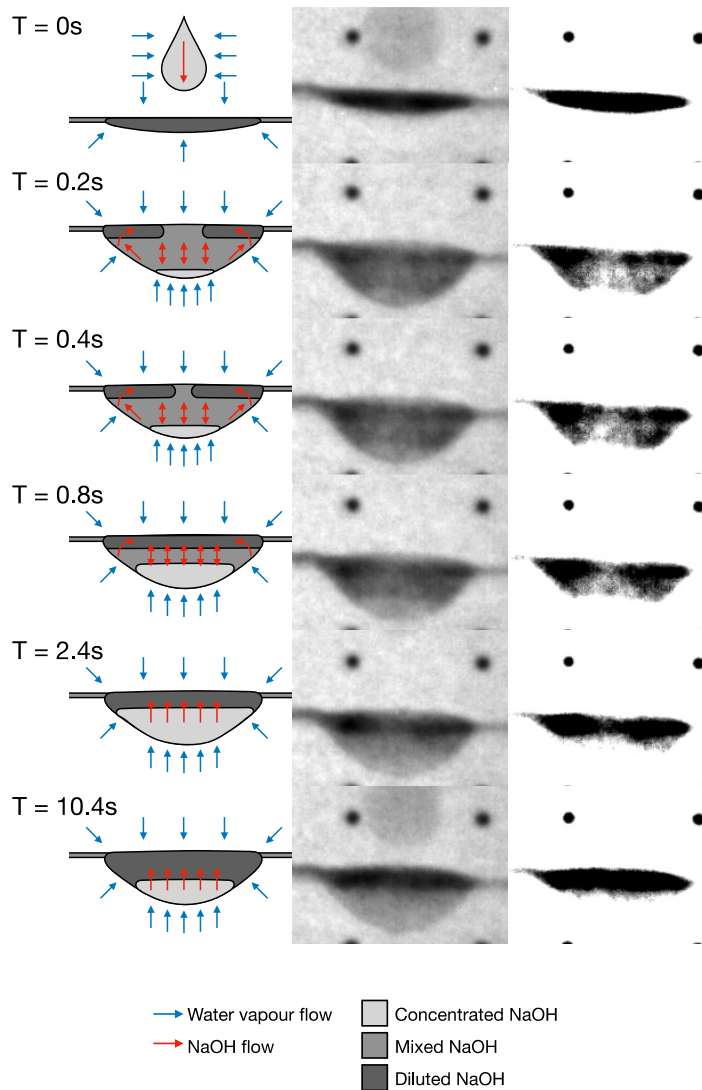
Figure 21: Image sequence of droplet suspension and impingement. Each step consists of a sketch, a normal image, and a contrast-enhanced image highlighting the dilute absorbent (black). The absorbent is suspended by attaching it to a wire mesh. A drop of fresh absorbent strikes the suspended drop. Initial mixing of the solution is rapidly followed by separation by stratification.

From this visualization, a potential to use the buoyance force movement from the varying specific mass of the absorbent was recognized. We proposed that if the absorption surface area was vertical, the water condensed on the surface would float over the charged, more dens absorbent. A method of vertically installed spiral finned tube with flooded fin spacing was developed. Figure 22 illustrates the idea.
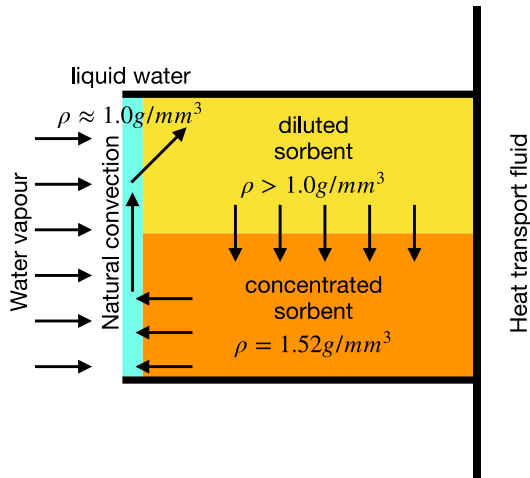
Figure 22: Illustration of the mass transport through buoyancy force.

3.3 Laboratory scale absorption heat and mass exchanger results

A variety of tests were conducted using a variation of vertically installed spiral fin tubes. It was found that realistic test temperatures were very important. Performance was much better at higher evaporating temperatures (non-realistic). This is due to the higher vapor density and higher absorption temperature, which leads to a significant reduction in fluid viscosity and thus improved mass transport in the film. Good functionality was found with a flooded finned tube made of copper, see Figure 23.
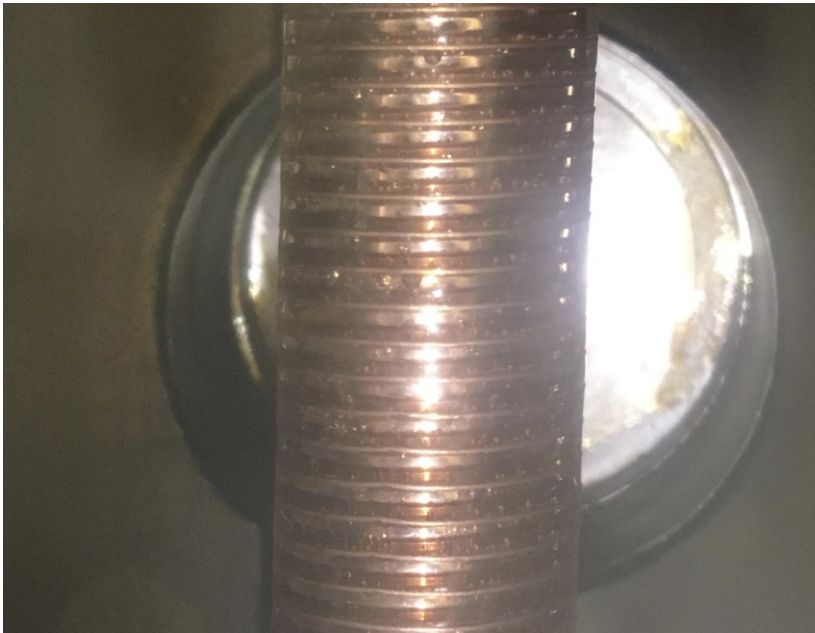

Figure 23: Image of the flooded finned tube made of copper, installed in the lab scale single tube heat and mass exchanger.

The results of the copper tube test were evaluated by plotting on the concentration vs. gross temperature lift diagram, which indicates the performance with respect to the material specific maximum. The evaluation is shown in Figure 24. The points aligned horizontally at the 50 wt% concentration indicate the resulting gross temperature lift and are compared to the equilibrium maximum. The values vertically aligned at 20K in the figure are compared to the minimum

29/44

concentration indicated by the equilibrium curve. The temperatures of the heat transfer fluids were measured and referenced. All tests shown are performed at an absorber inlet temperature of 25°C. Evaporator inlet temperatures are taken at 5°C (see Figures 24-26), 10°C (see Figure 27), and 15°C (see Figure 28) to provide a range of operation. When reading the diagram, a close match to the equilibrium state is generally sought, both in terms of maximum temperature gain for high outlet temperature and low concentration for maximum volumetric energy density. The absorber inlet and outlet temperatures can be calculated from the respective minimum and maximum gross temperature lift by adding the evaporator temperature. A guide to volumetric power and volumetric energy density can be obtained from the final concentration and mass flow. A decrease in final concentration with an increase in absorbent mass flow will result in greater power. The energy density, on the other hand, depends only on the final concentration, low concentration results in high energy density. For specific positioning, maximum and minimum volumetric power and energy values are provided in the graphs. Volumetric power is calculated with respect to the tube volume, excluding tube spacing, housing, or other system components, and volumetric energy density values are with respect to the volume in the charged state, including concentrated absorbent and absorbate (largest volume).

Figures 24 through 26 show graphs of typical operation with heat supplied by a geothermal heat exchanger at a supply temperature of 5°C. The tests reported were performed at absorbent flows of 6 g/min (Figure 24), 4 g/min (Figure 25), and 2 g/min (Figure 26). For all three absorbent flows, there was a clear pattern of greater temperature gain at low heat transfer fluid flow rates with high end concentration and low temperature gain at high heat transfer fluid flow rates with reduced end concentration.
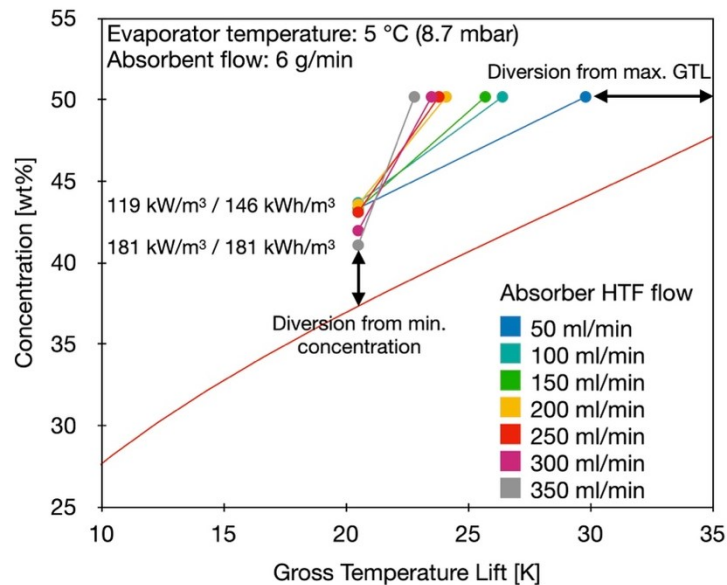

Figure 24: Concentration vs. Gross Temperature Lift plot comparing performance at 6 g/min absorbent flow, 5°C evaporator temperature, and varying heat transfer fluid flows to the equilibrium line.

Figure 25: Concentration vs. Gross Temperature Lift plot comparing performance at 4 g/min absorbent flow, 5°C evaporator temperature, and varying heat transfer fluid flows to the equilibrium line.

Figure 26: Concentration vs. Gross Temperature Lift plot comparing performance at 2 g/min absorbent flow, 5°C evaporator temperature, and varying heat transfer fluid flows to the equilibrium line.
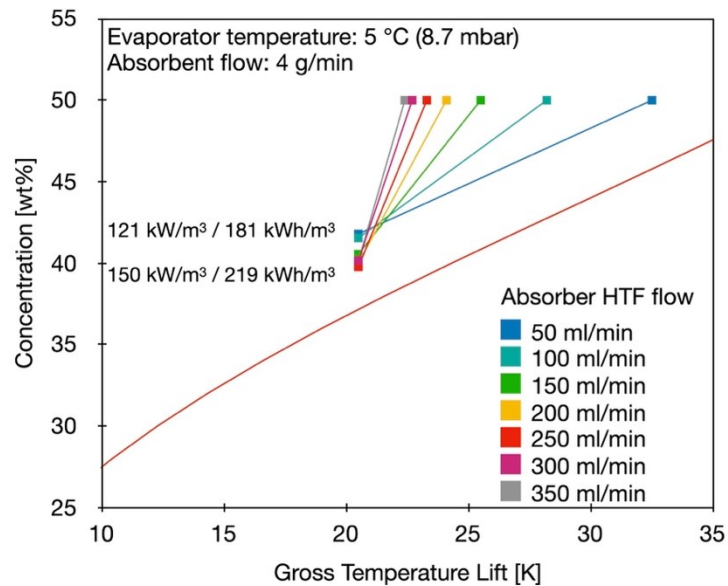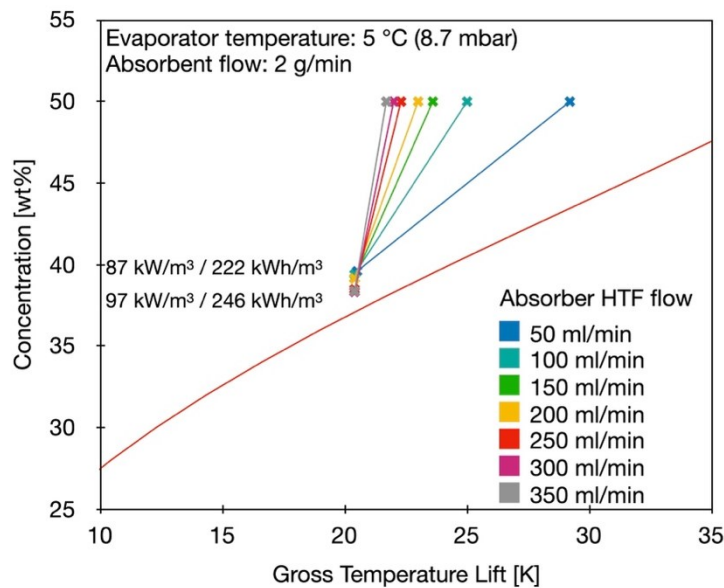
The results present the challenge of non-linear behavior between heat gain and temperature gain due to the concentration gradient, which comes from the non-linear nature of absorbent mass gain to concentration change. For this reason, more heat is available at low temperature gain (concentration decrease at lower initial concentration) than at higher temperature gain (concentration decrease at higher initial concentration). Since the heat capacity (J/kg) of the heat transfer fluid (water) is practically constant over the application temperature range, a high temperature gain can be achieved if its specific heat capacity (J/(kg K)) is equal to the absorbent heat capacity at high concentration change. On the other hand, low final concentration can only be achieved if the specific heat capacity of the heat carrier is adapted to the concentration change at low concentrations. The best volumetric power and volumetric energy density therefore depend on the required gross temperature lift, which in

turn depends on the required outlet temperature and the evaporator temperature. Figures 27 and 28 show examples of the same test conditions, but at different evaporator temperatures of 10°C and 15°C at constant absorbent flow. While the difference between the final concentration and the theoretical minimum concentration increases as the evaporating temperature increases, the specific concentration decreases significantly at low evaporating temperatures due to the increase in heat and mass transport (power).

High evaporating temperatures are much more favorable for both power and energy-based performance. The gross temperature lift is not as affected, but the final output temperature is of course since it is the sum of the gross temperature lift and the evaporating temperature. For this reason, if an output temperature of 35 °C is required for an underfloor heating system in a building, and a geothermal heat exchanger is used that provides heat at 5 °C, then the heat transfer fluid flow rate would need to be set between 50 ml/min and 100 ml/min per tube at an absorption flow rate of 4 g/min per tube. The volume specific power would then be just over 121 kW/m^3 and the volume energy capacity would be just over 181 kWh/m^3. On the other hand, if heat is available at 15 °C, a gross temperature increase of only 20 K would be required, so a flow between 150 ml/min and 200 ml/min per tube would be possible, allowing a volume specific power density of 330 kW/m^3 and a volume specific energy density of 340 kWh/m^3. These operating conditions could be made possible by operating in series with an air source heat pump. In this case, a first temperature increase from the air source heat pump is followed by a second step from the absorption heat storage system. This allows operation below 0°C heat source temperature, improves the storage capacity and allows the air source and absorption heat pump to reach a similar performance as the ground source heat pump.

Figure 27: Concentration vs. Gross Temperature Lift plot comparing performance at 4 g/min absorbent flow, 10°C evaporator temperature, and varying heat transfer fluid flows to the equilibrium line.
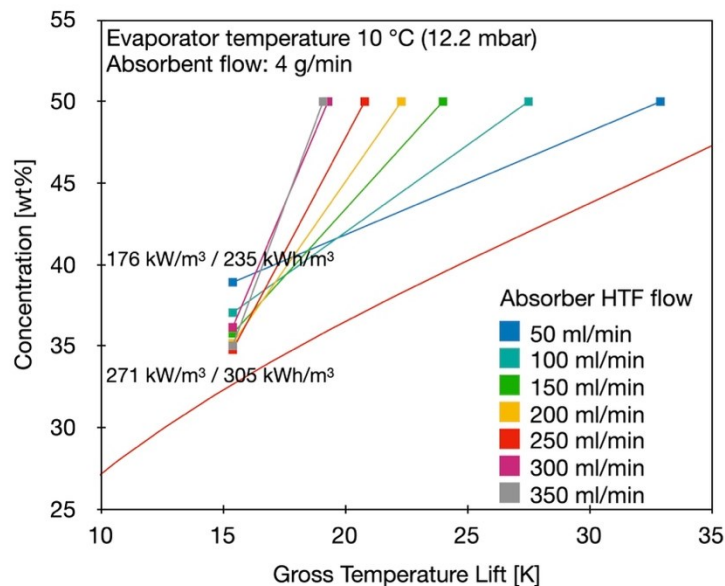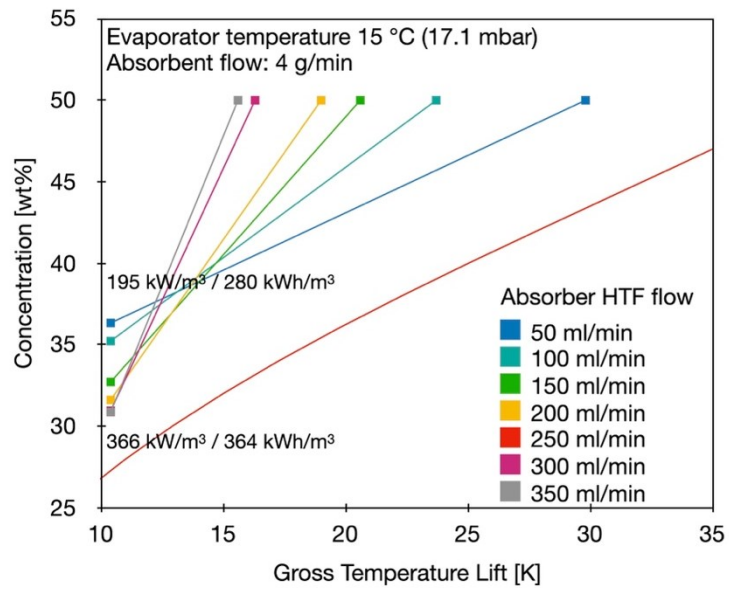
Figure 28: Concentration vs. Gross Temperature Lift plot comparing performance at 4 g/min absorbent flow, 15°C evaporator temperature, and varying heat transfer fluid flows to the equilibrium line.

3.4   Single-family home scale absorption heat storage results

Detailed dynamic absorption and desorption tests are performed according to the temperature guideline suggested in Chapter 3.6. While test results are obtained at steady state conditions, variation of test settings provides dynamic results for the test campaign. Power and energy density are measured at defined operating temperatures. For absorption, the absorber heat transfer input temperature is 30°C (25°C) and the output temperature is 35°C (30°C), and the evaporator input temperatures are tested from 20°C down to 4°C in 2K steps, with the output temperature 3K lower than the input. For desorption, the condenser inlet temperature is 30°C (20°C) and the outlet temperature is 5K higher, with desorber inlet temperatures varying from 49K to 55K higher than the condenser inlet temperature. Absorbent mass flow is taken at 2, 4 and 6 g/min per tube. Two pallet sized tanks are installed to contain the absorbent in charged and discharged state and 6 complete cycles are performed with 1200 kg of aqueous NaOH at 50 wt% concentration.

The results are shown in the following Figures 29 (absorption) and 30 (desorption), with temperature difference on the x-axis and energy density (relative to the absorber volume) and power on the y-axis for the absorption process and concentration and power for the desorption process.
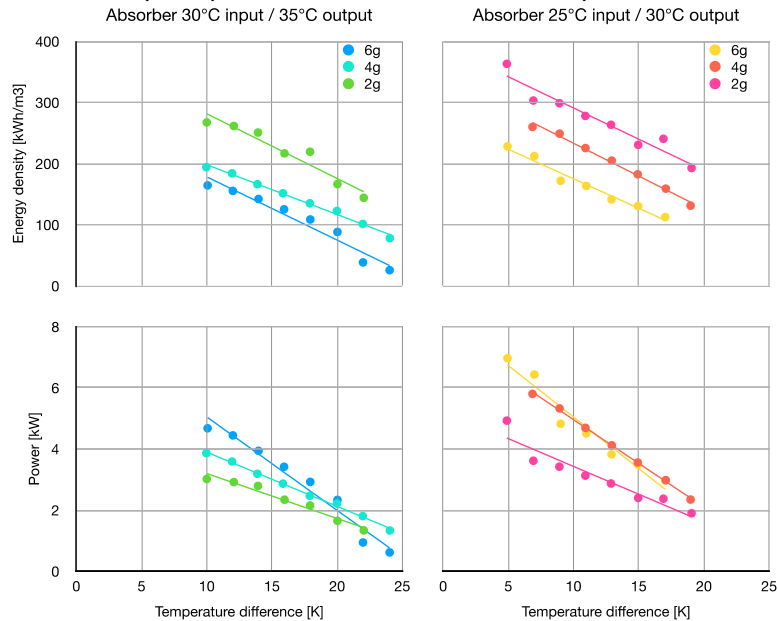

Figure 29: Plots showing energy density and power results from the absorption process at evaporator inlet temperatures of 20°C down to 6°C in 2K steps (x-axis shows temperature difference) and absorber inlet temperatures of 30°C and 25°C.
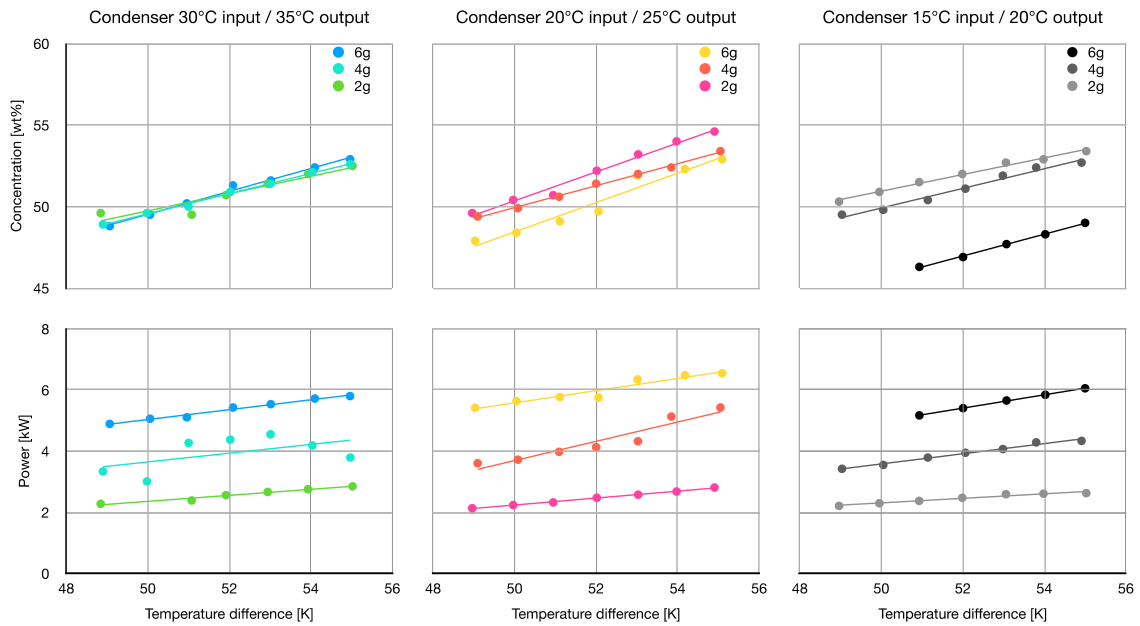
Figure 30: Plots showing concentration and power results from the desorption process at condenser inlet temperatures of 30°C, 25°C, and 15°C at temperature differences of 49K to 55K in 1K steps.

Under all testing conditions, stable operation was reached. In the absorption process, power and energy density strongly depends on the temperature difference between evaporator and absorber. Greater temperature difference reduces both power and energy density. Increased sorbent mass flow leads to greater power, but lower energy density. This is expected, since larger sorbent volume requires greater time to equilibrium. At an evaporator input temperature of 10°C, taken from the testing guideline, translating to a temperature difference at an absorber input temperature of 30°C (25°C) of 20K (15k), and an absorbent mass flow of 4g/min and tube, the energy density is at 123 kWh/m3 (182kWh/m3) and the power is 2.0kWh (3.8kW). In desorption, at an absorbent mass flow of 6g/min and tube, 50wt% concentration is reached at a temperature difference of 50K with a charging power of 5.5kWh. These results show the strong dependency of the system performance on the absorbent viscosity (temperature). For further optimization, measuring the concentration gradient along the spiral fin is central. One of the challenges recognized is the equal distribution of heat transport fluid in the spiral fin tube bundle and the respective equal distribution of the absorbent. This is a very important factor that needs to be advanced on.

3.5 Simulation of the sorption heat storage in a building results

Extensive work has been done on the dimensioning of the whole building heating system as described for single and multi-family houses in different climates, see Figure 31 for results on multi-family houses in Zurich at different system scales. The scale (scale multiplier) is a multiple of the single tube laboratory HMX (first spiral fin tests). The simulation work shows that for all parameters there is an upper limit to the system-dependent scale in terms of increased solar fraction and increased cost per kWh stored. Once sufficiently dimensioned, further increase in scale marginally increases the solar fraction at increasing cost of stored energy. There is a fixed upper limit to the collector, equal to the usable roof area defined by the building model. For buildings with high heat demand, this limitation affects the total solar fraction possible. For systems with high solar fraction (≥80%), increasing the solar collector area provides little benefit and increases the total system cost. For the buffer (hot water) tanks, there is a critical minimum size to exploit the short-term storage potential. Oversizing does not increase the solar fraction due to continuous thermal losses. There is a playoff between the solar collector area and the buffer tank. A parameter with a strong influence on the solar fraction is the scale multiplier (varying curves in Figure 31). This is due to the increase of the sorption heat storage power capacity. With a higher capacity, the solar collector heat peaks can be used more effectively for charging and the return temperature to the solar collectors is lower, which increases the collector efficiency. For the higher conversion capacity to be effective, the geothermal heat exchanger must be adequately sized. Otherwise, condensing and evaporating temperatures will negatively affect storage capacity, especially in the absorption process.
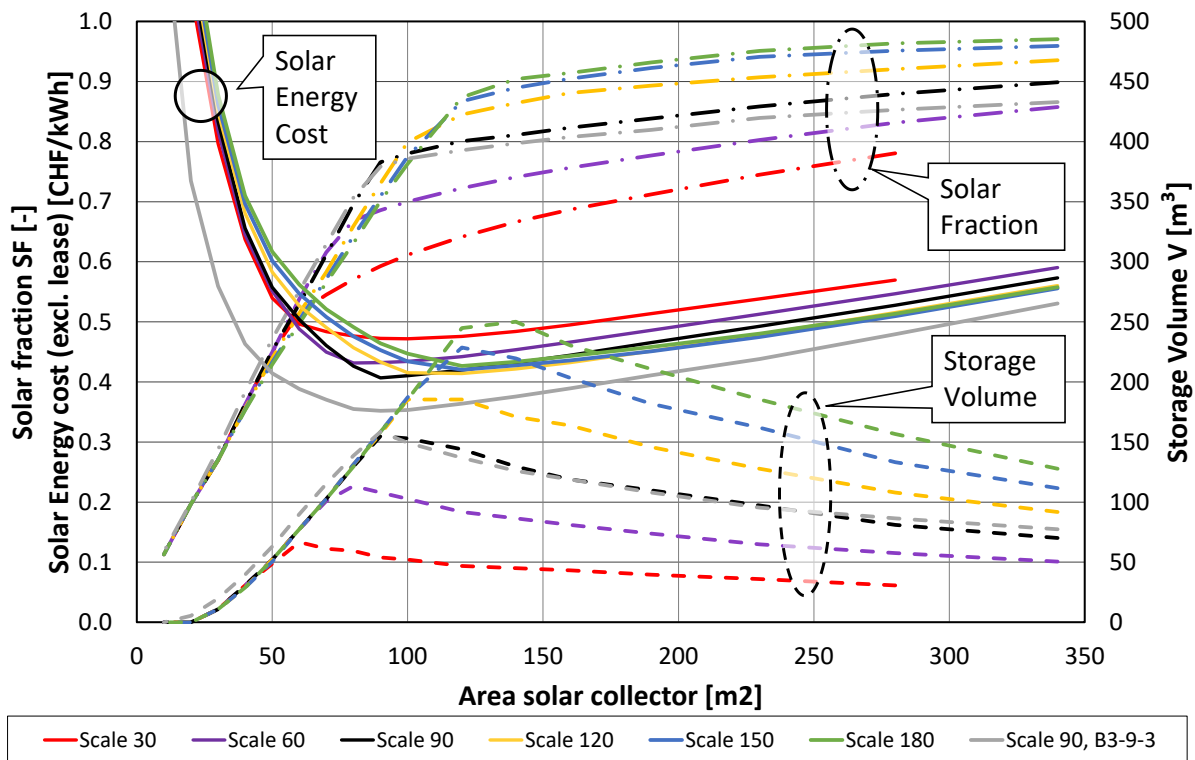

Figure 31: Variation of the scale multiplier and the solar collector Area for the multifamily home with 30kWh/m³a located in Zurich.

4   Conclusions

In this project, steps were taken from the analysis of the mass transport of water in aqueous sodium hydroxide to the design of a novel heat and mass exchanger and the construction of a single-family home scale sorption heat storage system. The challenge in the liquid absorption process for sorption heat storage is the slow mass transport of the absorbate, especially at low temperatures. This, combined with the need to achieve low concentrations during absorption (near equilibrium) for high energy density, led to the need to develop a new heat and mass exchanger design. The flooded spiral fin tube, as developed in this work, allows long exposure times due to the long absorbing flow path and shallow slope. Since the flow is strictly channelled, the accumulation of absorbent is prevented and good wetting at low absorbent flow is enabled. In addition, the vertical absorber surface is proposed to promote accelerated mass transport from the absorber surface to the bulk due to buoyancy force. Both the laboratory scale and single-family home scale heat and mass exchangers show good and stable performance, with nominal power and energy density of 4kW and 200kWh/m3, respectively.

The simulation results show that solar fractions above 80% can be achieved by incorporating long-term sorption storage. For the Zurich climate, sorption storage volumes of 100-250 m3 are required for MFH30. It was observed that increasing the size of one system component often resulted in another component becoming the new bottleneck, requiring further adjustments.

In addition to the specific research on heat and mass exchanger design, this project has contributed to the sorption heat storage research community by categorizing the different processes, defining test temperatures to enable comparison, and introducing a method for performance mapping.

5   Outlook and next steps

This work has attracted considerable interest. In collaboration with a Swiss industrial partner and supported by the Swiss Climate Foundation, preparatory work for the development of a marketable product is underway.

In order to evaluate the potential of this long term heat storage technology in a wide range of applications, a new model based on the current knowledge and results is needed. An application has been submitted to the Swiss Federal Office of Energy for this purpose. The work will focus in particular on the combination of compression heat pump and sorption heat storage and will consider the aspects of winter electrical load reduction, operation scheme and customer benefits.

An additional field demonstration project is being developed in collaboration with industry to further advance the technology and demonstrate operation in a building-integrated environment.

An internal HSLU project proposal in collaboration with the School of Art and Design has been approved to investigate the storage design with respect to user acceptance.

Further research to be addressed includes:

In this project, a substantial technical step in the storage of renewable energy for building space heating and domestic hot water has been achieved, including the extensive preparation for next development and implementation steps.

6   National and international cooperation

National cooperation:

With the University of Applied Sciences Rapperswil (HSR) within the framework of the SCCER Heat and Electricity Storage.

With the Empa Laboratory of Advanced Analytical Technologies in the field of Raman spectroscopy and neutron imaging.

With the PSI SINQ neutron imaging facility in the frame of the neutron imaging performed.

With the AEE Suisse, "Forum Energiespeicher Schweiz" FESS in the working group for thermal energy storage in collaboration with ETHZ, PSI, HSLU, HSR.

International cooperation:

There is a strong international exchange within the IEA SHC 58 / ES 33 Task and the ongoing SHC 67 / ES 40 Task, as well as within the TCM storage community in general.

With the University of Ulster as well as the University of Warwick in the framework of the completed PhD Thesis.

7 Publications

Scientific publications:

[1] Fumey, B., Weber, R., Baldini, L., "Heat transfer constraints and performance mapping of a closed liquid sorption heat storage process", Applied Energy, Volume 335, 2023, 120755

[2] Borgschulte A, Terreni J, Fumey B, Sambalova O and Billeter E "Short-Lived Interfaces in Energy Materials" Front. Energy Res. 9:784082. doi: 10.3389/fenrg.2021.784082

[3] Fumey,B., Baldini,L., Static Temperature Guideline for Comparative Testing of Sorption Heat Storage Systems for Building Application. Energies 2021, 14, 3754. https://doi.org/10.3390/en14133754

[4] Fumey B., Borgschulte A., et al. Enhanced gas-liquid absorption through natural convection studied by neutron imaging, International Journal of Heat and Mass Transfer 182 (2022) 121967

[5] Baldini, L., Fumey, B., "Seasonal Energy Flexibility Through Integration of Liquid Sorption Storage in Buildings", Energies 2020, 13, 2944.

[6] Fumey, B., Baldini, L. and Borgschulte, A., "Water Transport in Aqueous Sodium Hydroxide Films for Liquid Sorption Heat Storage", Energy Technol., Volume 8, 2020, 2000187.

[7] Fumey B., Weber R., Baldini L., "Sorption based long-term thermal energy storage – Process classification and analysis of performance limitations: A review", Renewable and Sustainable Energy Reviews 111, 2019, 57–74

[8] Fumey B., Weber R., Baldini L., Liquid sorption heat storage – A proof of concept based on lab measurements with a novel spiral fined heat and mass exchanger design, Applied Energy, Volume 200, 2017, 215-225

[9] Fumey B., Weber R., Baldini L., "Cycling test of liquid sorption thermal energy storage using sodium hydroxide", SWC/SHC Conference Abu Dhabi United Arab Emirates, 2017.

University Semester Projects:

Sorptionswärmespeicher, Erprobung, Bewertung und Charakterisierung der Labor-Demonstrationsanlage, Güntensperger, J., 2022, PAIND

Bachelor Thesis:

[1] Sorptions-Wärmespeicher - Statische Betriebsevaluation, Krummenacher, M., 2022, Bachelor Thesis, http://portfoliodb.hslu.ch/entries/cf032c3d-6be4-4e21-bd39-d6f67911efe6

[2] Auslegung von einem Sorptionswärmespeicher für ein Mehrfamilienhaus, Güntensperger, J., 2023.

PhD Thesis:

Heat and Mass Exchanger Design for Inter-seasonal Liquid Absorption Heat Storage, Fumey, B. May 2020, Doctoral Thesis, https://pure.ulster.ac.uk/en/studentTheses/heat-and-mass-exchanger-design-for-inter-seasonal-liquid-absorpti

Conference presentations:

[1] Component development for a liquid sorption TES system, ISES SHC webinar, 2019.

[2] Thermochemical material testing under semi-real conditions: A lab-scale bulk reactor to support optimised component design for long-term thermal energy storage, IRES, Dusseldorf, Germany, 2019.

[3] Einblick in die Entwicklung von Wärmespeicher mit flüssigen Sorbentien, Fachforum Thermische Energiespeicher, Meerbusch / Düsseldorf, Germany, 2019

[4] Liquid sorption heat storage spiral fin heat and mass exchanger, steps towards increased rate of absorption, 12th International Renewable Energy Storage Conference IRES, Dusseldorf, Germany, 2018.

[5] Cycling test of liquid sorption thermal energy storage using sodium hydroxide, SWC/SHC Abu Dhabi United Arab Emirates, 2017.

Other publications:

[1] Fumey B., et al. "Material and Component Development for Thermal Energy Storage: Objectives and Outlook", Solar Update, 2017.

Newspaper articles:

[1] Wärmespeicher, Was steckt in der Lauge?, Nachrichten aus der Chemie, 70, April 2022

[2] Wärme aus dem Laugentank, Haustech 11, 2019

[3] Heizen statt abschalten, Technology review, 2018

[4] Sommerwärme für die Wintersaison, Empa Quarterly, 2017.

[5] Wärmespeicher mit Natronlauge, Haustech, 11, 2017.

[6] Die Sommerwärme in den Winter retten, NZZ, 2017.

[7] IEA SHC Task 58: "We will need new and innovate designs for heat and mass exchangers", Solar Thermal World, 2017.

[8] Wie retten wir die Sonnenwärme in den Winter?, Spectrum der Wissenschaft, 2017.

[9] Die Lösung im rechten Rohr, Tec21, 2017

TV reports:

[1] 3Sat, Nano, Fertig ist die Lauge - Heizen mit erneuerbaren Energien funktioniert nur mit Wärmespeicher. Eine Möglichkeit: Natronlauge, 2018

International Energy Agency participation:

SHC Task 58 / ES Annex 33: Material and Component Development for Thermal Energy Storage

Serving as Leader for Subtask 4T "Component design for Thermo Chemical Materials"

- 1st Experts Meeting, April 5-7, 2017, Lyon, France
- 2nd Experts Meeting, October 4-6, 2017, Dubendorf, Switzerland
- 3rd Experts Meeting, April 9-11, 2018, Ljubljana, Slovenia
- 4th Experts Meeting, October 1-2, 2018, Graz, Austria
- 5th Experts Meeting + Public Seminar, May 1-3, 2019, Otttawa, ON, Canada
- 6th Experts Meeting, October 9-11, 2019, Messina, Italy

SHC Task 67 / ES Annex 40: Compact thermal energy storage; materials within components within systems

Serving as Leader for Subtask E-TCM "Effective Component Performance with Innovative Materials"

- 1st Experts Meeting, October 27-29, 2021, Vitoria-Gasteiz, Spain
- 2nd Experts Meeting, April 4-5, 2022, Graz, Austria
- 3rd Experts Meeting, September 29-30, 2022, Kassel, Germany

8   References

[1]   Wang R, Zhai X. Handbook of energy systems in green buildings. ISBN978-3-662- 49185-0. Springer-Verlag Berlin Heidelberg; 2018.

[2]   International Energy Agency Solar Heating and Cooling Programme (IEA SHC). Task 58. Advanced thermal storages - towards higher energy densities, long term storage and broader operating ranges. 2018. p. 12–4.

[3]   Stutz B, Le Pierres N, Kuznik F, Johannes K, Barrio EPD, B´ed´ecarrats J-P, et al. Storage of thermal solar energy. Comptes Rendus Phys 2017;18:401–14. https://doi.org/10.1016/j.crhy.2017.09.008.

[4]   Baldini, L., Fumey, B., "Seasonal Energy Flexibility Through Integration of Liquid Sorption Storage in Buildings", Energies 2020, 13, 2944.

[5]   van Helden W, Yamaha M, Rathgeber Ch, Hauer A, Huaylla F, Le Pierrès N, Stutz B, Mette B, Dolado P, Lazaro A, Mazo J, Dannemand M, Furbo S, Campos-Celador A, Diarce G, Cuypers R, König-Haagen A, Höhlein S, Brüggemann D, Fumey B, Weber R, Köll R, Wagner W, Daguenet-Frick X, Gantenbein P, Kuznik F. IEA SHC task 42/ ECES Annex 29 – working group B: applications of compact thermal energy storage. Energy proced 2016;91:231–45.

[6]   International Energy Agency. Energy technology perspectives report. 2016978-92- 64-25233-2.

[7]   Hadorn JC. IEA solar heating and cooling programme—task 32: advanced storage concepts for solar and low energy buildings. Proceedings of ECO- STOCK. 2006.

[8]   Rathgeber, Ch. Hiebler, S. Lävemann, E. Dolado, P. Lazaro, A. Gasia, J. de Gracia, A. Miró, L. Cabeza, LF. König-Haagen, A. Brüggemann, D. Cam- pos-Celador, A. Franquet, E. Fumey, B. Dannemand, M. Badenhop, T. Diriken, J. Nielsen, JE. Hauer, A. (2016). IEA SHC task 42/ECES Annex 29 – a simple tool for the economic evaluation of thermal energy storages. Energy Procedia. 91, pp. 197–206.

[9]   Tatsidjodoung, P. Le Pierrès, N. Luo, L. A review of potential materials for thermal energy storage in building applications, Renewable and Sustainable Energy Reviews, Volume 18, 2013, Pages 327-349.

[10]   Kabus, F. and Wolfgramm, M. (2009). Aquifer thermal energy storage in Neubrandenburg - Monitoring throughout three years of regular operation. EFFSTOCK'2009. In: 11th International Conference on Thermal Energy Storage, Stockholm, Sweden.

[11]   Dannemand, M. Johansen, JB. Kong, W. Furbo, S. (2016). Experimental in- vestigations on cylindrical latent heat storage units with sodium acetate trihydrate composites utilizing supercooling. Applied Energy. 177, pp. 591–601.

[12]   Englmair, G. Moser, Ch. Furbo, S. Dannemand, M. Fan, J. (2018). Design and functionality of a segmented heat-storage prototype utilizing stable supercooling of sodium acetate trihydrate in a solar heating system. Ap- plied Energy. 221, pp. 522–534.

[13]   Zondag, HA. (2015). Chapter 6 - Sorption Heat Storage, Editor(s): Bent Sørensen, Solar Energy Storage, Academic Press. pp. 135-154.

[14]   Fumey,B. ,Baldini,L. Static Temperature Guideline for Comparative Testing of Sorption Heat Storage Systems for Building Application. Energies 2021, 14, 3754. https://doi.org/10.3390/en14133754

[15]   Haghighat F. Energy storage with energy efficient buildings and districts: optimization and automation. Tech. rep. 2018.

[16]   Vasiliev, LL. and Kulakov, AG. (2003). Heat Pipe Applications in Sorption Re- frigerators. In: Kakaç S., Smirnov H.F., Avelino M.R. (eds) Low Tempera- ture and Cryogenic Refrigeration. NATO Science Series (Series II: Mathe- matics, Physics and Chemistry), vol 99. Springer, Dordrecht.

[17]   Inglezakis, VJ. and Poulopoulos, S. (2006). Adsorption, ion exchange and catalysis: design of operations and environmental applications. Elsevier.

[18]   Perry, RH. (2007) Perry's chemical engineers' handbook. eighth ed. Mc Grawhill.

[19]   Garg, HP. Mullick, SC. Bhargava, AK. (1985). Solar thermal energy storage. Dordrecht: Reidel Publishing Company.

[20]   Kawasaki, H. Watanabe, T. Kanzawa, A. (1999). Proposal of a chemical heat pump with paraldehyde depolymerization for cooling system. Applied Thermal Energy. 19(2), pp. 133–43.

[21]   Boman, BD. Hoysall, DC. Staedter, MA. Goyal, A. Ponkala, MJ. Garimella, S. (2017a). A method for comparison of absorption heat pump working pairs. International Journal of Refrigeration. 77, pp. 149–175.

[22]   Aristov, YI. (2013). Challenging offers of material science for adsorption heat transformation: a review. Applied Thermal Engineering. 50(2), pp. 1610– 1618.

[23]   N'Tsoukpoe, KE. Le Pierrès, N. Luo, L. (2013). Experimentation of a LiBr- H2O absorption process for long-term solar thermal storage: prototype design and first results. Energy 53, pp. 179–98.

[24]   Cabeza, LF. Solé, A. Barreneche, C. (2017). Review on sorption materials and technologies for heat pumps and thermal energy storage. Renewable Energy, 110, pp. 3–39.

[25]   Hauer A. Sorption theory for thermal energy storage. In: Paksoy HÖ., editor. Thermal energy storage for sustainable energy consumption. Netherlands: Springer; 2007. p. 393–408.

[26]   Bales, C. (2005). Thermal Properties of Materials for Thermo-chemical Stor- age of Solar Heat. A Report of IEA Solar Heating and Cooling programme – Task. 32. 2005.

[27]   Kato, Y. (2007). Chemical energy conversion technologies for efficient energy use, Thermal energy storage for sustainable energy consumption. Springer Netherlands. pp. 377–91.

[28]   Wang, LW. Wang, RZ. Oliveira, RG. (2009). A review on adsorption working pairs for refrigeration. Renewable and Sustainable Energy Reviews. 13(3), pp. 518–534.

[29]   Srivastava, NC. Eames, IW. (1998). A review of adsorbents and adsorbates in solid- vapour adsorption heat pump systems. Applied Thermal Engi- neering. 18(9–10), pp. 707–714.

[30]   Armstrong, F. Blundell, K. (2007). Energy ... beyond oil. Oxford University Press.

[31]   N'Tsoukpoe KE, Liu H, Le Pierrès N, Luo L. A review on long-term sorption solar energy storage. Renew Sustain Energy Rev 2009;13(9):2385–96.

[32]   Kuznik F, Johannes K, Obrecht Ch, David D. A review on recent developments in physisorption thermal energy storage for building applications. Renew Sustain Energy Rev 2018;94:576–86.

[33]   Palomba V, Frazzica A. Recent advancements in sorption technology for solar thermal energy storage applications. Sol Energy 2018. in press.

[34]   Solé A, Martorell I, Cabeza LF. State of the art on gas–solid thermochemical energy storage systems and reactors for building applications. Renew Sustain Energy Rev 2015;47:386–98.

[35]   Yu N, Wang RZ, Wang LW. Sorption thermal storage for solar energy. Prog Energy Combust 2013;39:489–514.

[36]   Abedin AH, Rosen MA. A critical review of thermochemical energy storage systems. Open Renew Energy J 2011;4:42–6.

[37]   Fumey B., Weber R., Baldini L., "Sorption based long-term thermal energy storage – Process classification and analysis of performance limitations: A review", Renewable and Sustainable Energy Reviews 111, 2019, 57–74

[38]   Zondag H, Kikkert B, Smeding S, de Boer R, Bakker M. Prototype thermochemical heat storage with open reactor system. Appl Energy 2013;109:360–5.

[39]   Kerskes H, Mette B, Bertsch F, Asenbeck S, Drück H. Development of a thermo-chemical energy storage for solar thermal applications. Proceedings of ISES solar world congress. 2011.

[40]   Weber R, Asenbeck S, Kerskes H, Drück H. SolSpaces – testing and performance analysis of a segmented sorption store for solar thermal space heating. Energy proced 2016;91:250–8.

[41]   van Alebeek R, Scapino L, Beving MAJM, Gaeini M, Rindt CCM, Zondag HA. Investigation of a household-scale open sorption energy storage system based on the zeolite 13X/water reacting pair. Appl Therm Eng 2018;139:325–33.

[42]   Tatsidjodoung P, Le Pierrès N, Heintz J, Lagre D, Luo L, Durier F. Experimental and numerical investigations of a zeolite 13X/water reactor for solar heat storage in buildings. Energy Convers Manag 2016;108:488–500.

[43]   Weber R, Dorer V. Long-term heat storage with NaOH. Vacuum 2008;82(7):708–16.

[44]   Fumey B., Weber R., Baldini L., Liquid sorption heat storage – A proof of concept based on lab measurements with a novel spiral fined heat and mass exchanger design, Applied Energy, Volume 200, 2017, 215-225

[45]   Köll R, van Helden W, Engel G, Wagner W, Dang B, Jänchen J, Kerskes H, Badenhop T, Herzog T. Experimental Investigation of a realistic scale seasonal solar sorption storage system for buildings. Sol Energy 2017;155:388–97.

[46]   Zondag H, Kalbasenka A, van Essen M. First studies in reactor concepts for thermochemical storage. Proceedings of the Eurosun. 2008.

[47]   Mette B, Kerskes H, Drück H. New high efficient regeneration process for thermo- chemical energy stores. Proceedings of innostock. 2012.

[48]   Boman DB, Hoysall DC, Pahinkar DG, Ponkala MJ, Garimella S. Screening of working pairs for adsorption heat pumps based on thermodynamic and transport characteristics. Appl Therm Eng 2017;123:422–34.

[49]   Mette B, Kerskes H, Drück H. Concepts of long-term thermochemical energy storage for solar thermal applications – selected examples. Energy proced 2012;30:321–30

[50]   Goldstein M. Some physical chemical aspects of heat storage. In: UN Conf. New Sources Energy, Rome (Italy); 1961. http://digitallibrary.un.org/recor d/3828050. [Accessed 19 December 2020].

[51]   M. Goldstein, Some physical chemical aspeets of heat storage: Goldstein, Martin, United National Conference on new sources of energy, Rome, 1961, 17 p., Sol Energy 7 (2) (1963) 84. doi:10.1016/0038-092X(63)90029-X.

[52]   International Energy Agency, Solar Heating and Cooling Programm, Task 42: https://task32.iea-shc.org

[53]   International Energy Agency, Solar Heating and Cooling Programm, Task 42: https://task42.iea- shc.org

[54]   International Energy Agency, Solar Heating and Cooling Programm, Task 58: https://task58.iea- shc.org

[55]   International Energy Agency, Solar Heating and Cooling Programm, Task 67: https://task67.iea- shc.org

[56]   Kokouvi Edem N'Tsoukpoe, Frederic Kuznik, A reality check on long-term thermochemical heat storage for household applications, Renewable and Sustainable Energy Reviews 139 (2021) 110683

[57] Weber, R. and V. Dorer, *Long-term heat storage with NaOH.* Vacuum, 2008. **82**(7): p. 708-716.

[58] Fumey B., Weber R., Gantenbein P., Daguenet-Frick X., Stoller S., Fricker R., Dorer V., "Operation results of a closed sorption heat storage prototype", Energy Procedia Volume 73, 2015, Pages 324-330

[59] Analyse des schweizerischen Energieverbrauchs 2000–2020 nach Verwendungszwecken, Oktober 2021, bfe.admin.ch

[60]   Villasmil Willy, Troxler Marcel, Hendry Reto, Worlitschek Jörg. OPTSAIS – Exergetic and economical optimization of seasonal thermal energy storage systems. Luzern: HSLU; 2019.

[61]   Fumey B, Weber R, Gantenbein P, Daguenet-Frick X, Williamson T, Dorer V. Development of a Closed Sorption Heat Storage Prototype. Energy Procedia 2014;46:134–41. https://doi.org/10.1016/j.egypro.2014.01.166.

[62]   Preise - Deutsch n.d. https://www.jenni.ch/preise.html (accessed October 21, 2021).

[63]   Mit Erdsondenbohrungen Kosten sparen | Bauen und Wohnen in der Schweiz 2018. https://bawos.ch/erdsondenbohrungen-kosten-und-planung-zur-gewinnung-von-umgebungswaerme/ (accessed October 21, 2021).

[64]   Energie 360°. Allgemeine Offerte für den Erdsondenbau in NEST 2014.

[65]   Lager mieten in Zürich | homegate.ch n.d. https://www.homegate.ch/mieten/lager/ort-zuerich/trefferliste (accessed October 21, 2021).